NASA Technical Memorandum 81932

An Investigation of Radiometer Design Using Digital Processing Techniques

Roland W. Lawrence

January 1981

National Aeronautics and Space Administration

Langley Research Center
Hampton, Virginia 23665

TABLE OF CONTENTS

LIST OF TABLES

LIST OF FIGURES

FIGURE PAGE

CHAPTER I

INTRODUCTION

The search for natural resources, the need for accurate weather prediction, as well as many other scientific studies have stimulated widespread interest in remote sensing devices. One such device is the microwave radiometer. The radiometer has proven valuable in remotely determining the physical temperature of surfaces, thickness of sea and lake ice, salinity of seawater, and the location of oil spills. The radiometer may be able to determine these physical properties by measuring the power level of the electromagnetic energy emitted from the object. The energy emitted by the object is actually a very low level gaussian random variable with zero mean [4]. Estimating the variance of this signal presents several interesting problems. One problem is that the actual power level of the received signal may be lower than the receiver noise power. Because of the extremely low level of these signals, substantial amplification is required before any attempt can be made to measure the power level of the received signal. The amplifiers used to provide this gain must be very stable since changes in the gain will cause error in the measured power of the received signal. Thus, in order to measure the power of the received signal accurately, the receiver noise and the gain of the radiometer must be precisely known and extremely stable. Any uncertainty in the receiver noise power or the gain results in erroneous measurement of the power of the signal and thus will degrade the quality of the measurement of physical properties.

The Dicke switching noise injection radiometer shown in figure 1-1 is one system used to estimate the power level of the received signal while reducing errors due to the previously mentioned problems. An introduction to the basic operation of this radiometer can be found in Appendix A and also in references [4], [5], and [7]. Referring to figure 1-1, the received signal is modulated by switching between a reference noise source and the antenna output. This Dicke switching strategy eliminates the effect of the receiver noise on the measurement of the received signal. The noise injection or feedback scheme eliminates the effect of gain fluctuation on this measurement. A Dicke switching noise injection radiometer of this type has been developed by R. F. Harrington at NASA Langley Research Center. Since construction of the radiometer, advances in understanding and interpretation of radiometric data have necessitated further refinements in the existing system.

The objective of this research is to investigate techniques for improving the power measurement performance of the existing Dicke switching noise injection radiometer. The general approach of this investigation will be to develop an analytical model of the existing radiometer. It will be shown from this model that the use of sample data techniques leads to an improved power estimation strategy.

A model of the existing radiometer will be developed and analyzed in Chapter II. From this analysis features which adversely affect the power estimate performance of the radiometer will be identified. In the first section of Chapter III, this model is used to develop a sample data processing approach which will improve the power estimate performance

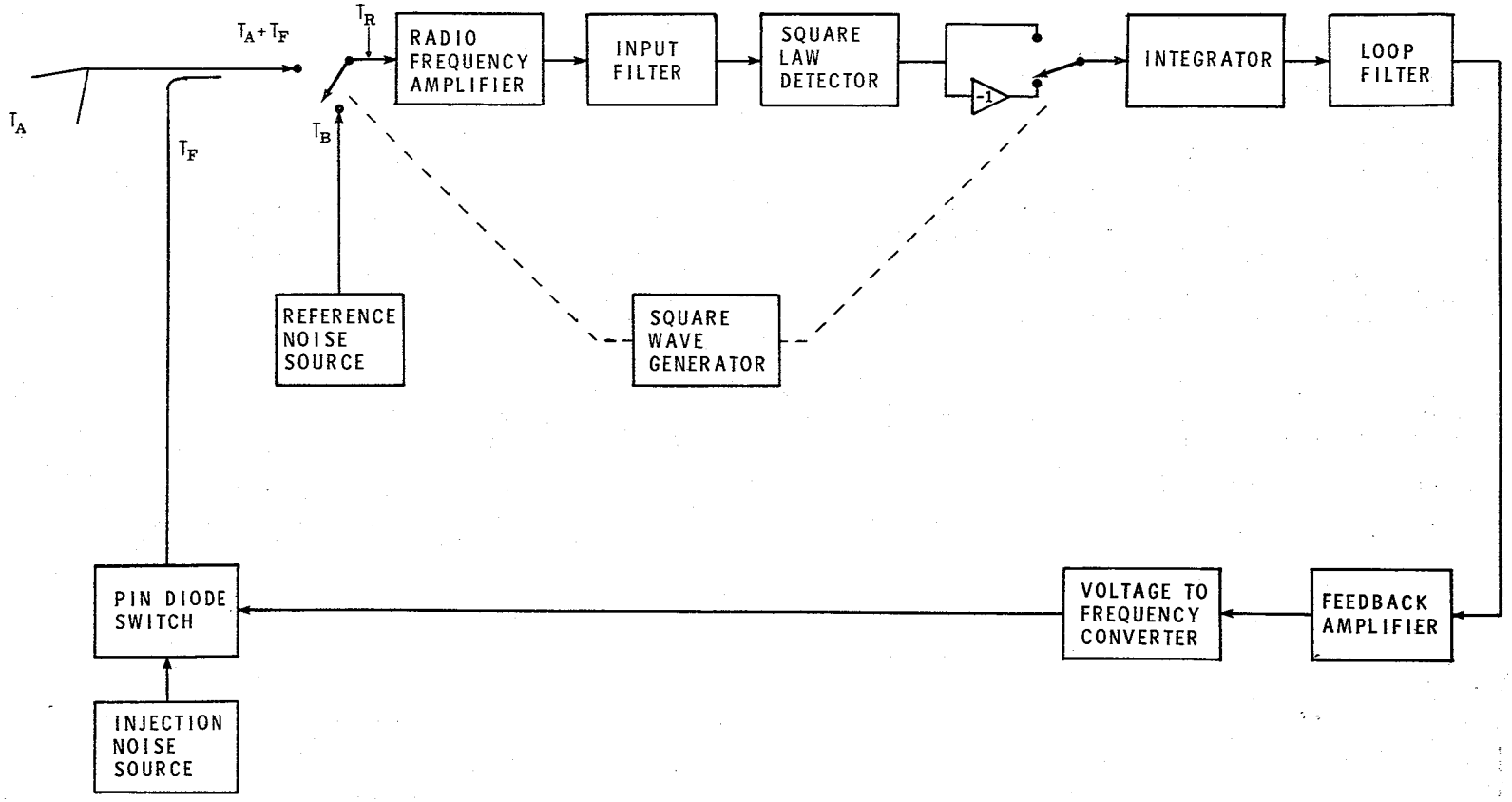

Figure 1-1. Dicke switching noise injection radiometer.

of the radiometer. The second section of Chapter III deals with the details of implementing the design improvements. The results of an analysis using the developed model and the proposed processing technique, as well as preliminary experimental results obtained via a prototype design using an Intel 8086 microprocessor, are presented in Chapter IV. Conclusions drawn from these results are contained in Chapter V.

CHAPTER II

DEVELOPMENT OF RADIOMETER MODEL

In this chapter an analytical model will be developed for the existing Dicke switching noise injection radiometer. Several performance parameters of the radiometer, such as sensitivity and measurement time, will be defined. From the analytical model, expressions for these performance parameters will be obtained. Methods of improving the power measurement performance of the radiometer will then be discussed.

A block diagram of the existing radiometer is shown in figure 2-1. The system consists of five major sections: the antenna subsystem, the microwave front end, the detector, the video amplifier, and the analog signal processor. Of interest here is the development of a model to be used in subsequent analysis of the entire radiometer. In order to evolve such a model, the transfer functions of the various sections must be determined. To provide continuity of presentation, several brief descriptions of the subsystems are presented. A detailed analysis of these subsystems has been performed and can be found in reference [10]. In the following development of the radiometer model, the signal and noise power components will be represented by their respective effective temperatures. The basis for this representation is developed in Appendix A. Henceforth, the term effective temperature will be used to refer to a corresponding power. The brightness temperature of an object will be used to refer to the temperature corresponding to the power received by the antenna.

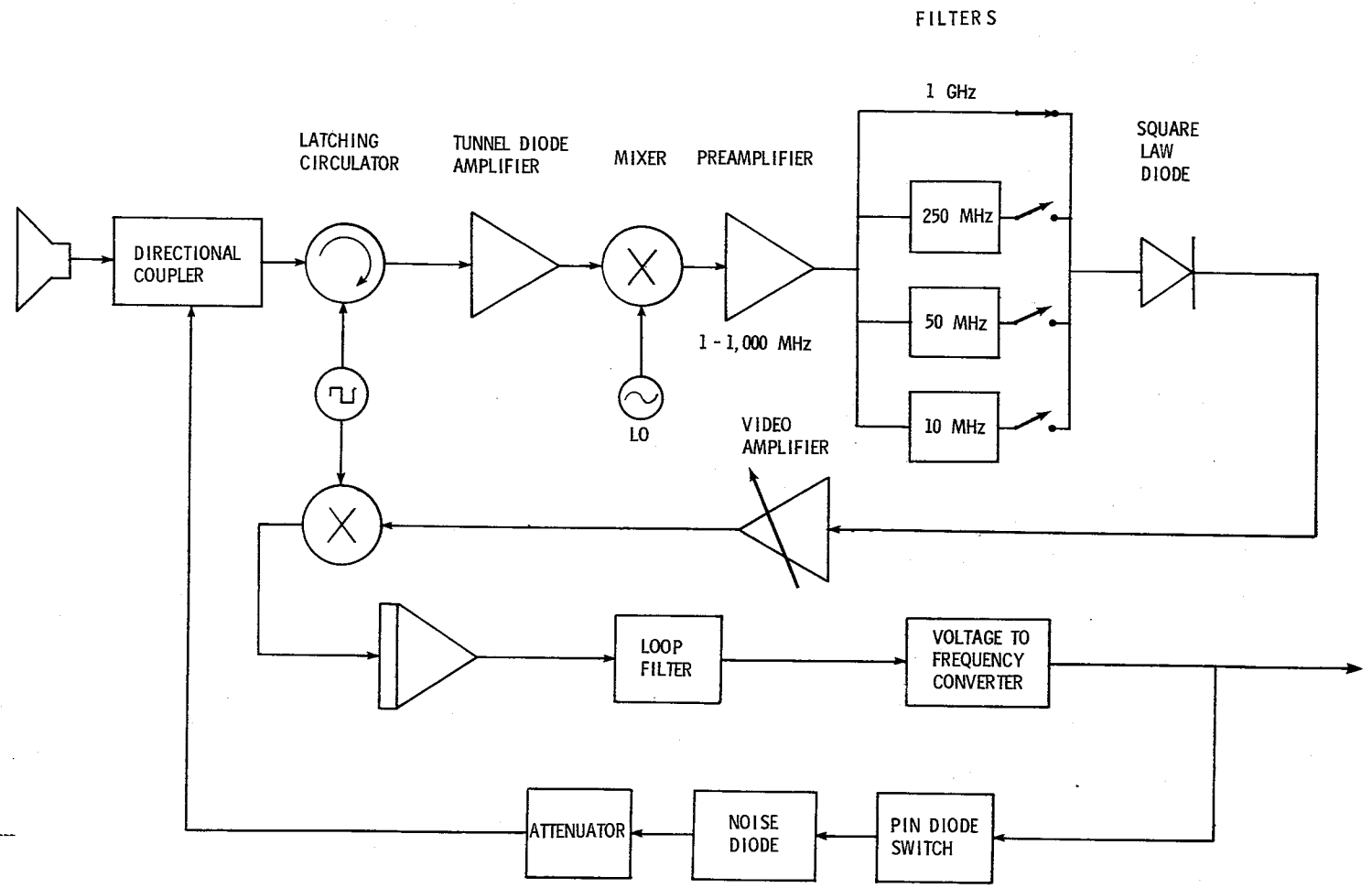

Figure 2-1. Block diagram of existing radiometer.

A. Development of Analytical Model

Referring to figure 2-1, the antenna subsystem collects the incident electromagnetic radiation and feeds it to the microwave front end. The feedback noise is also injected into the microwave front end and is added to the received signal. The circulator alternately switches the input of the tunnel diode amplifier between the received signal and the injected noise combination and the reference noise. The output of the tunnel diode amplifier is down converted to zero intermediate frequency (i.e., dc homodyne receiver) and amplified further by the mixer preamplifier. This entire microwave section of the radiometer is housed in a constant temperature enclosure. The reference noise is provided by a matched load also within the enclosure. Thus, the physical temperature of the microwave components and the reference temperature are both at the enclosure temperature of 308 K. This eliminates the need to accurately measure the ohmic losses within the microwave front end. The frequency response of the microwave front end is sufficiently broad that the effect of this portion of the system can be represented by a constant power density gain factor. This gain bandwidth constant was determined to be 137.63 dB·Hz [10].

The output of the microwave front end is filtered and detected by the detector section. The filter bank of figure 2-1 establishes the effective input statistical bandwidth which will be of importance in later analysis. Since changing this input filter will clearly change the power applied to the square-law detector, attenuators are included in the filter bank to assure that the power applied to the detector is

the same for all filters. The output of the square-law diode is a linear function of the input power. Measurements indicated that the gain constant of this square-law detector is 400 V/W [10].

The relatively low level square-law detector output is then amplified by the video amplifier. This amplifier should pass virtually all components of the Dicke switch frequency with minimum attenuation and phase shift. The amplifier need not pass dc since the mean of the temperature estimate appears as a modulated component of the Dicke frequency. Thus, the amplifier should display substantial attenuation at low frequencies to reduce flicker or 1/f noise. This video amplifier has been analyzed [10], and the transfer function was found to be

$$G_V(s) = \frac{0.693(1 + 2.39s)s^2}{\left[1 + s/(2\pi \times 2.41)\right]\left[1 + s/(2\pi \times 2.01)\right]} \times \frac{1}{\left[1 + s/(2\pi \times 0.3)\right]\left[1 + s/(2\pi \times 5.03 \times 10^3)\right]} \qquad (2\text{-}1)$$

An analysis of the Bode plot of this function revealed that the video amplifier is relatively flat from above a few hertz to about 5 or 6 kHz.

The output of the video amplifier is applied to the correlator, which effectively demodulates the signal restoring the dc value. The output of the correlator is then applied to the analog signal processor or estimation and averaging section. The analog processor must estimate the mean or dc level of the output of the demodulator switch. This

estimation section consists of an integrator and a loop filter. The transfer function for this combination was determined to be

$$G_p(s) = \frac{-196.4\left[1 + s/(2\pi \times 62.525)\right]}{s\left[1 + s/(2\pi \times 5.684)\right]} \qquad (2\text{-}2)$$

The final constant required to form the complete transfer function of the radiometer is the feedback constant determined by the noise injection process. The noise injection is accomplished by the use of a voltage-to-frequency converter producing constant width pulses with a frequency directly proportional to the output voltage of the analog processor. The output pulses of the voltage-to-frequency converter control a PIN [13] diode switch which is used as a gate controlling the noise diode. The noise diode excess noise temperature, or noise above ambient temperature, is specified by the manufacturer to be 31 dB above 290 K, corresponding to an excess noise temperature of approximately 365,000 K. The voltage-to-frequency converter produces an output of 863 pulses/second per volt. Each pulse is 70 μs wide; thus, the duty cycle is given by

$$d = (863)(70 \times 10^{-6})\ V_o \qquad (2\text{-}3)$$

$$d = 0.0604\ V_o$$

where V_o is the voltage output of the estimation and averaging section. These injected noise pulses are attenuated by a 6 dB attenuator and then added to the antenna noise via a 20 dB directional coupler. The noise diode and attenuator are both included in the constant temperature

enclosure with the microwave front end. Thus, they have a physical temperature equal to the reference temperature, i.e., 308 K. Consider the effect of the 6 dB attenuator on the feedback noise temperature. The output of an attenuator at a physical temperature T_P with input noise temperature T_{IN} can be shown to be

$$T_N = LT_{IN} + (1 - L)T_P \tag{2-4}$$

where L is the power loss factor ($L < 1$). The input to the attenuator is the total noise diode temperature $T_D = T_{EX} + T_B$. Therefore, since the attenuator is within the constant temperature enclosure, equation (2-4) can be written as

$$\begin{aligned} T_N &= 0.25T_D + (1 - 0.25)T_B \\ T_N &= 0.25(T_{EX} + T_B) + (1 - 0.25)T_B \\ T_N &= 0.25T_{EX} + T_B. \end{aligned} \tag{2-5}$$

Thus, an equivalent model for the feedback can be obtained by including only the excess noise temperature of the noise diode and adding the reference temperature at the output of the attenuator. Using this method, the feedback mechanism shown in figure 2-2 is obtained.

The feedback model of figure 2-2 can be combined with the system constants calculated earlier to form the block diagram model of the radiometer shown in figure 2-3. The input bandwidth determined by the filter bank of figure 2-1 need not be considered in the control loop analysis. However, its effect on the operation of the radiometer will

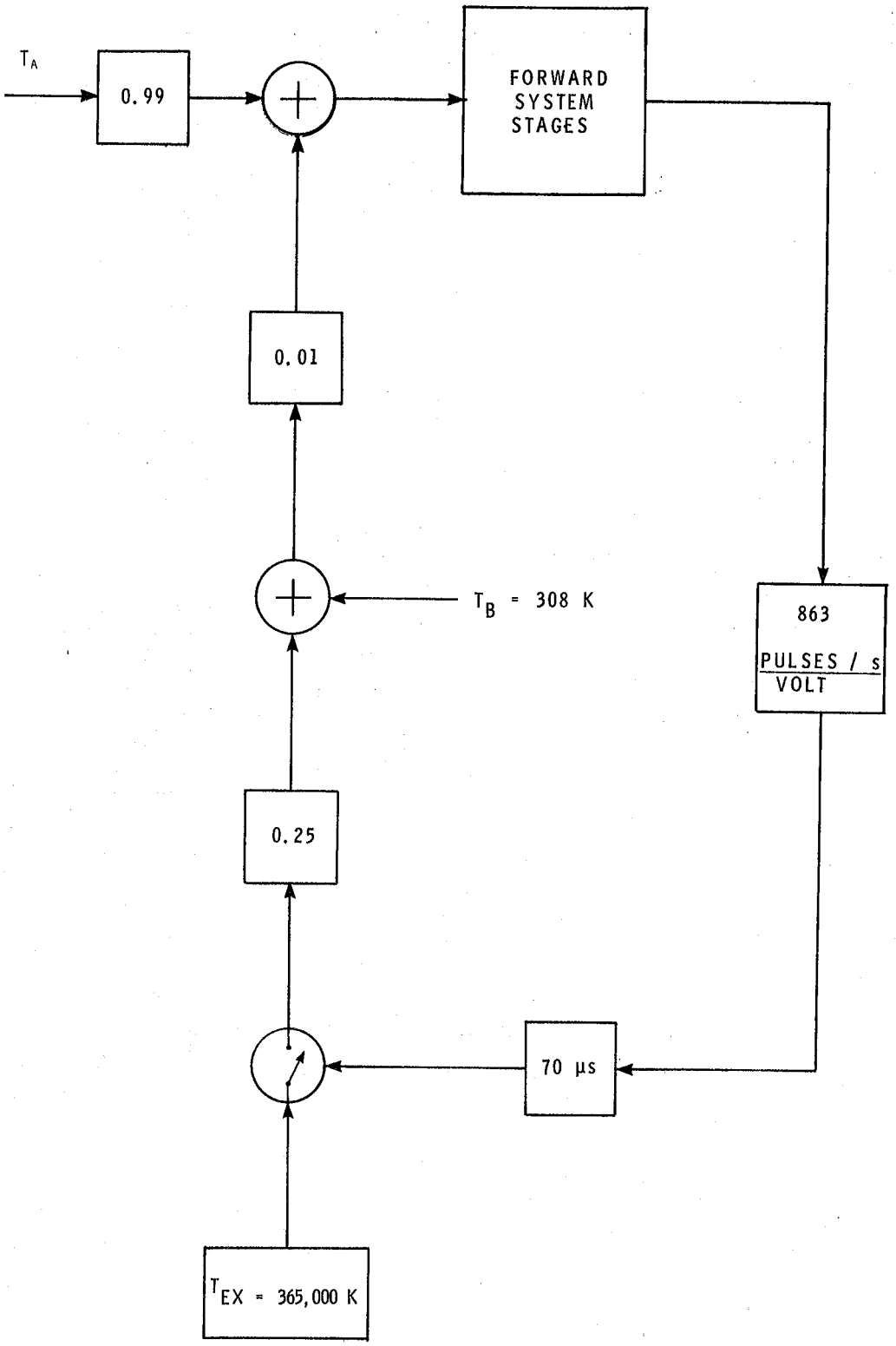

Figure 2-2. Illustration of noise addition model.

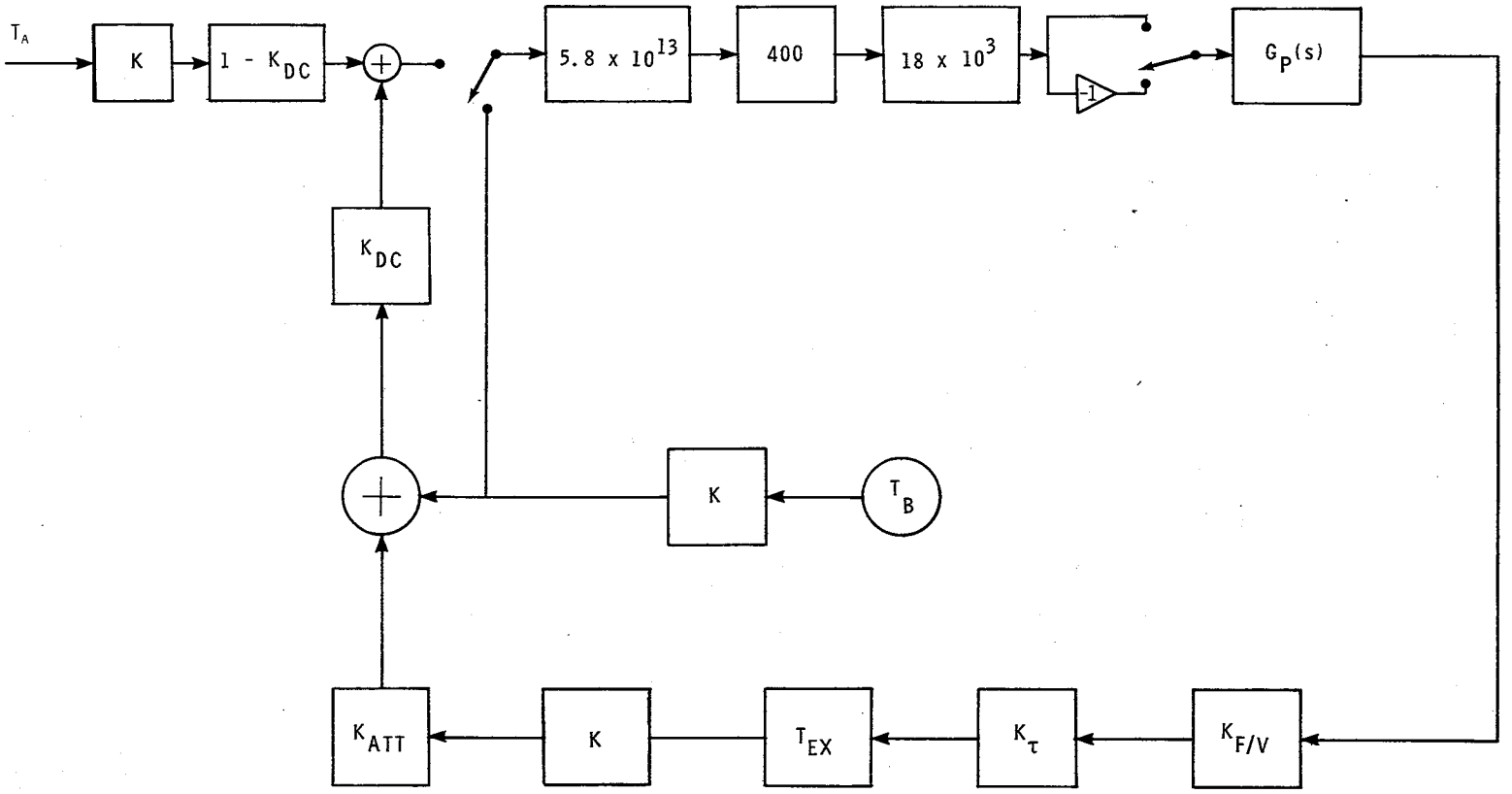

Figure 2-3. Model of present radiometer system.

be considered later. Note also that the frequency response of the video amplifier is assumed to be sufficiently broad not to affect the control loop, and it is represented by its pass band gain.

The control loop of figure 2-3 can be simplified by first combining the feedback constants, then moving Boltzmann's constant within the control loop, and finally combining the gain constants in the forward loop. A further simplification is obtained by representing the switching process with only one switch. This is possible since fluctuations in the frequency response of the system between the first switch and the correlator switch occur at such high frequencies that they can be neglected for control loop analysis. With these simplifications, the control model illustrated in figure 2-4 is obtained, where the 0.5 factor is due to the Dicke switching process.

Before analyzing this model, an important point about the feedback pulses and the video amplifier should be noted. The assumption was made that the frequency response of the video amplifier was sufficiently broad to be neglected in the control loop analysis. However, the amplifier is not broadband enough to pass the narrow feedback pulses without some distortion. Proper operation of the Dicke switching process requires that all noise injected into the antenna portion of the Dicke cycle appear in the antenna portion at the correlator switch. Any energy that "spills over" due to bandwidth limitation between the switches will result in an error in the measurement process. It was determined that the bandwidth of the video amplifier was insufficient to process the noise injection pulses without some "spillover" error. This error was

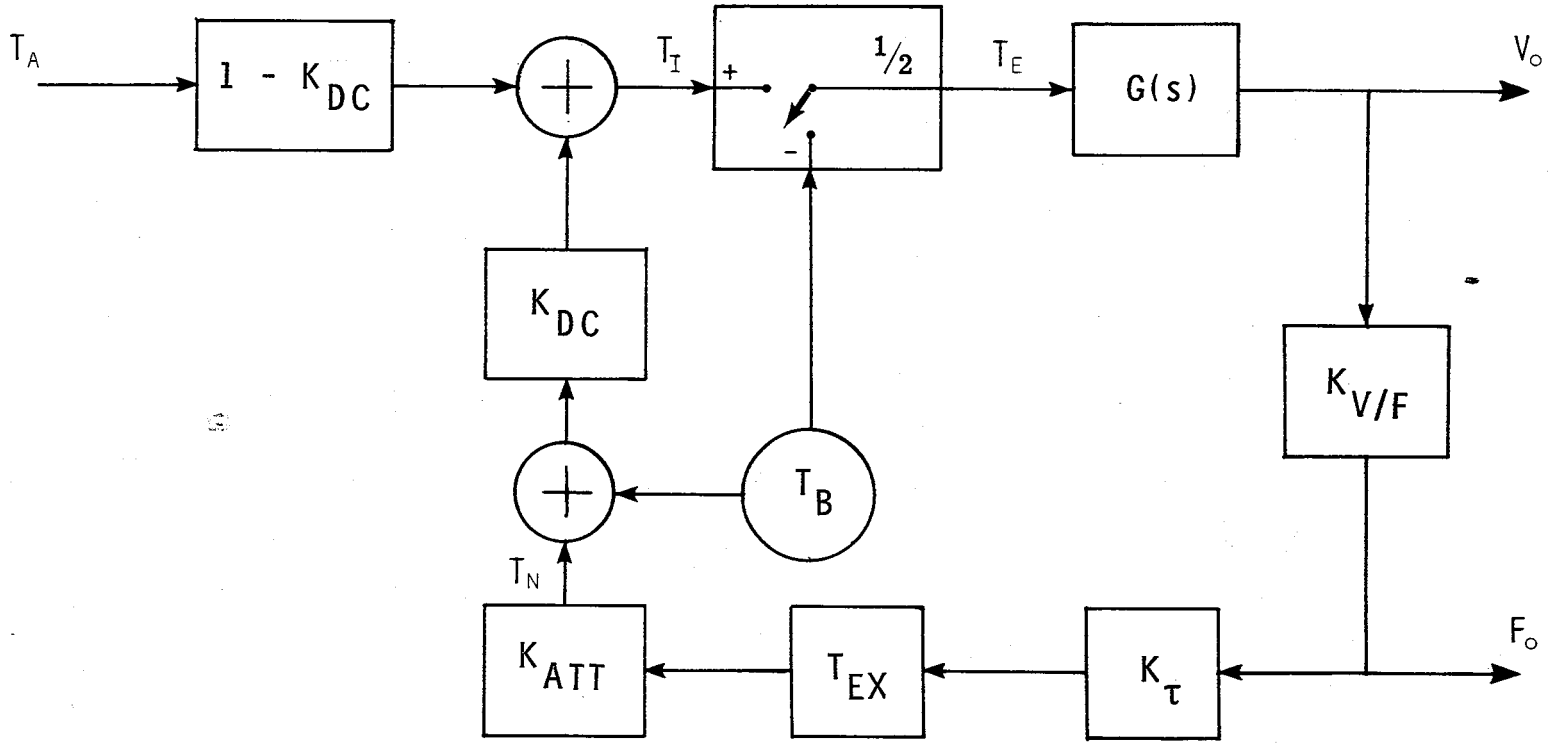

Figure 2-4. Control model of present system.

observed qualitatively using computer simulation of the radiometer. The error has also been measured during calibration of the radiometer [10].

An analysis of the control model of figure 2-4 will now be conducted in order to develop a closed-loop transfer function for the present radiometer. The noise temperature T_E of figure 2-4 is given by

$$T_E = 0.5(T_I - T_B) \tag{2-6}$$

where T_I is the effective output temperature of the directional coupler and T_B is the reference temperature. The effective output temperature of the directional coupler can be seen from figure 2-4 to be

$$T_I = (1 - K_{DC})T_A + K_{DC}(T_B + T_N) \tag{2-7}$$

where T_N is the injected noise appearing at the attenuator output. The noise temperature at the attenuator output is given by

$$T_N = K_{ATT}T_{EX}K_1V_o \tag{2-8}$$

where K_{ATT} is the attenuator constant, T_{EX} is the excess temperature of the noise diode, and $K_1 = K_{V/F}K_\tau$ is the constant relating the output voltage to the duty cycle of the injected noise pulses. The output voltage $V_o(s)$ can be expressed as

$$V_o(s) = -G(s)T_E. \tag{2-9}$$

Substituting equations (2-6), (2-7), and (2-8) into (2-9) results in the following expression for $V_o(s)$:

$$V_o(s) = -\frac{1}{2}G(s)(T_I - T_B)$$

$$V_o(s) = -\frac{1}{2}G(s)\left[(1 - K_{DC})T_A + K_{DC}(T_B + T_N) - T_B\right]$$

$$V_o(s) = -\frac{1}{2}G(s)\left[(1 - K_{DC})T_A + K_{DC}(T_B + K_{ATT}T_{EX}K_1V_o) - T_B\right] \qquad (2\text{-}10)$$

$$V_o(s) = -\frac{1}{2}G(s)\left[(1 - K_{DC})(T_A - T_B) + K_{DC}K_{ATT}T_{EX}K_1V_o\right]$$

where the term $K_{DC}K_{ATT}T_{EX}K_1V_o$ is the feedback noise. The transfer function relating $V_o(s)$ to $T_B - T_A$ can be determined from equation (2-10) to be

$$G_{CL}(s) = \frac{V_o(s)}{T_B - T_A}$$

$$G_{CL}(s) = \frac{\frac{1}{2}G(s)(1 - K_{DC})}{1 + \frac{1}{2}G(s)K_{DC}K_{ATT}T_{EX}K_1} \qquad (2\text{-}11)$$

Substituting the proper values into (2-11) results in

$$G_{CL}(s) = \frac{\frac{1}{2}(0.99)(1.132)\left[\frac{1 + 2.545 \times 10^{-3}s}{s(1 + 28 \times 10^{-3}s)}\right]}{1 + \frac{1}{2}(0.99)(1.132)\left[\frac{1 + 2.545 \times 10^{-3}s}{s(1 + 28 \times 10^{-3}s)}\right]55.12} \qquad (2\text{-}12a)$$

$$G_{CL}(s) = \frac{20.0(1 + 2.545 \times 10^{-3}s)}{s^2 + 38.52s + 1103.1} \qquad (2\text{-}12b)$$

The poles of this transfer function are readily determined to be $s = -19.26 \pm j27.06$. Thus, the damping factor is $\alpha = 19.26$, and the

damped radian frequency is $\omega_d = 27.06$ rad/s. The undamped natural radian frequency is $\omega_o = 33.21$ rad/s. The damping ratio $\zeta = \alpha/\omega_o = 0.580$. This closed-loop transfer function can be used to analyze several aspects of the radiometer's performance.

B. Analysis of Model

A thorough understanding of exactly what the radiometer is measuring and how this measurement relates to the brightness temperature are essential in attempting to properly interpret the results obtained using the previously developed model. As explained in Appendix A, the output of the square-law detector is a random process with mean proportional to the brightness temperature of the scene within the antenna footprint. Let $y(t)$ be this process, and let

$$y(t) = \mu_y(t) + z(t) \tag{2-13}$$

where $z(t)$ is a random process with zero mean, and $\mu(t)$ is the mean value of $y(t)$ corresponding to the brightness temperature within the antenna footprint. The brightness temperature of the scene $B(t)$ is then determined by

$$B(t) = E\{y(t)\} \tag{2-14}$$

where $B(t)$ is the brightness temperature of the scene within the antenna footprint versus time. Since it is not practical to have a large number of radiometers measuring the same scene in order to form the ensemble average of equation (2-14), the radiometer must use a time

average of the output of the square-law detector as an estimator of the brightness temperature. It is shown in Appendix B that this time average is not an unbiased estimator of the brightness temperature, but it is an estimate of the average brightness temperature of the scene covered by the path of the antenna footprint in τ seconds. Thus, longer integration times will produce a more accurate estimate of the average brightness temperature of a larger area. If, however, more spatial resolution of the actual brightness temperature is required, longer integration times may not provide more accuracy. If the time average is used as an estimator of $B(t)$, and if the integration time is comparable to the antenna footprint dwell time, a bias error results. This error was calculated in equation (B-4) and is repeated here for convenience.

$$e_{ANT} = \sum_{n=1}^{\infty} \frac{B^{(2n)}(t)\,\tau^{2n}}{(2n)!(2n+1)(2^{2n})} \tag{2-15}$$

This bias error or "antenna smear" error is due to the antenna footprint movement and subsequent changing of the brightness temperature during the integration time. It should be noted that the bias error of equation (2-15) is a function of the brightness temperature. Thus, the level of the "antenna smear" error will depend on the type of scene being measured.

As the analog processor forms the required time average and produces an estimate of the brightness temperature, the random nature of the process causes fluctuations in the estimate. The sensitivity of a

radiometer is an indicator of the level of these fluctuations. The sensitivity ΔT of a radiometer is defined as the amount by which the input temperature must be changed to result in the output estimate changing by one standard deviation. The sensitivity of a closed-loop square wave correlated Dicke radiometer can be shown to be [12].

$$\Delta T = 2(T_R + T_B)\sqrt{\frac{2B_{NO}}{B_{SI}}} \tag{2-16}$$

where T_R and T_B are the receiver and reference noise temperatures, respectively, B_{SI} is the effective input statistical bandwidth, and B_{NO} is the output equivalent noise bandwidth. Thus, in order to determine the sensitivity of the radiometer, the output equivalent noise bandwidth must be known.

The equivalent one sided noise bandwidth of the radiometer is defined by

$$B_{NO} = \frac{1}{G_{CL}^2(o)} \int_0^\infty |G_{CL}(f)|^2 df \tag{2-17}$$

where $G_{CL}(f)$ is the response of the control model given in equation (2-12). It can be shown [10] that the equivalent one sided noise bandwidth for the transfer function of (2-12) is given by

$$B_{NO} = \left[\frac{1 + (\omega_o \tau_2)^2}{8\zeta}\right]\omega_o \tag{2-18}$$

where τ_2 is the time constant of the lead portion of the loop filter and ω_o is the undamped natural radian frequency. Substituting the appropriate values from equation (2-12) into equation (2-18) results in

$$B_{NO} = \left[\frac{1 + (33.21 \times 2.545 \times 10^{-3})^2}{8(0.580)}\right]33.21$$

$$B_{NO} = 7.21 \text{ Hz}. \tag{2-19}$$

Substituting this value for B_{NO} as well as 308 and 627 K for T_B and T_R, respectively, into equation (2-16), the following result is obtained:

$$\Delta T = 2(627 + 308)\sqrt{\frac{2(7.21)}{B_{SI}}}$$

$$\Delta T = 1870\sqrt{\frac{14.42}{B_{SI}}} \tag{2-20}$$

The various sensitivities as a function of different input bandwidths were calculated using equation (2-20), and the values for the four available system input bandwidths are summarized in table 2-1.

TABLE 2-1

SENSITIVITY AND REQUIRED MEASUREMENT TIME

FOR PRESENT RADIOMETER

B_{SI}		20 MHz	100 MHz	500 MHz	2 GHz
ΔT		1.59 K	0.710 K	0.317 K	0.159 K
τ_S		0.393 s	0.409 s	0.419 s	0.511 s

There is a settling time associated with the loop parameters used to obtain the output noise bandwidth of equation (2-19). In order to determine this settling time or the time required to form an estimate, the transient response of the loop to a step input must be obtained. The step response of the present radiometer can be obtained by multiplying equation (2-12b) by the Laplace transform of a step function and taking the inverse transform. The step response $y(t)$ is determined to be

$$y(t) = C(T_B - T_A)\left[1 - 1.17e^{-19.26t} \sin (27.06t + 0.956)\right] \qquad (2\text{-}21)$$

Clearly, the error $\Delta y(t)$ due to the loop settling time is

$$\Delta y(t) = C(T_B - T_A)(1.17)e^{-19.26t} \sin (27.06t + 0.956) \qquad (2\text{-}22)$$

If the settling time is defined as the time required for the settling error to be less than 10 percent of the fluctuation of the estimate ΔT, then equation (2-22) can be written as

$$\frac{\Delta T}{10} = (T_B - T_A)(1.17)e^{-19.26t} \sin (27.06t + 0.956) \qquad (2\text{-}23)$$

where ΔT is the sensitivity of the measurement and τ_s is the time required to make the measurement. When determining the maximum settling time from equation (2-23), the peaks due to the overshoot phenomena must be considered. The time at which these peaks occur can be found by

taking the derivative of equation (2-23) and setting it equal to zero. This yields

$$t_{max} = \frac{1}{27.06}\left[\frac{\pi(2n - 1)}{2} - 0.956\right] \qquad n = 1,2,3,... \qquad (2\text{-}24)$$

The settling time was calculated for each input bandwidth using equations (2-23) and (2-24), and these results are presented in table 2-1. Increasing this settling time will decrease the fluctuations ΔT, but will also increase the possibility of "antenna smear" error. Thus, for optimum performance the radiometer should form the estimate to the required sensitivity in the shortest possible integration time.

In addition to the noise fluctuations and "antenna smear" error in the output of the loop, there is an error component due to the Dicke switching process. This so-called Dicke ripple is due to the modulation and demodulation processes within the Dicke radiometer. Consider the block diagram of figure 2-5. If it is assumed that the loop has reached steady state and if the feedback pulses are represented by their average level, the voltage waveform of 2-5 is obtained for the output of the correlator. Since this waveform has odd symmetry, it has no even harmonics and the magnitudes of the odd numbered Fourier components are readily determined to be

$$V_N = \frac{4}{N\pi} K_1(T_B + T_R)\left|G(jN\omega_d)\right| \qquad (2\text{-}25)$$

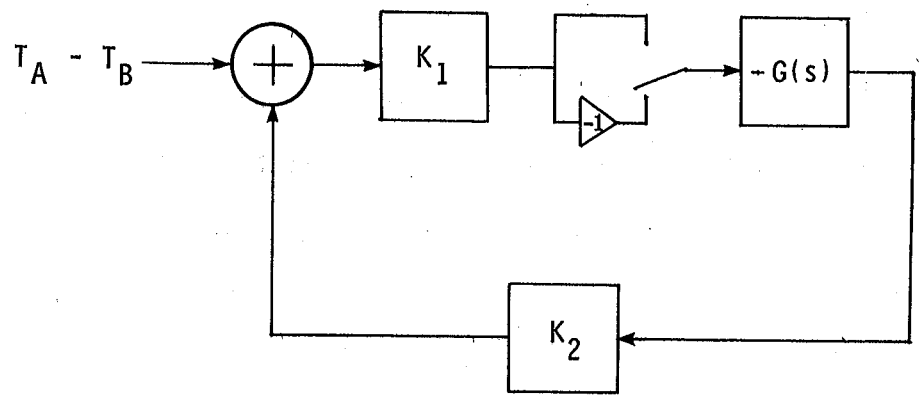
$T_A - T_B$
K_1
-1
$-G(s)$
K_2

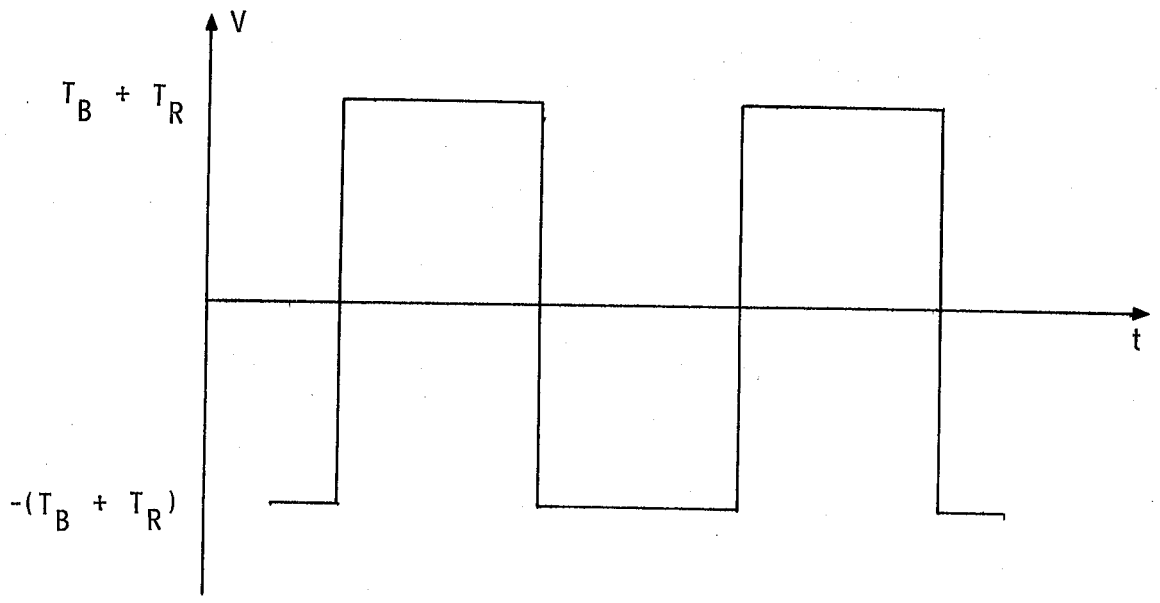
V
$T_B + T_R$
$-(T_B + T_R)$
t

where ω_d is the radian Dicke frequency. The dc level V_o with the loop in steady state is given by

$$V_o = \frac{T_B - T_A}{K_2} \tag{2-26}$$

For typical loop parameters, the fundamental component V_1 is usually much larger than the higher order components. Thus, the assumption that the total Dicke ripple level can be approximated by V_1 will be made. This assumption was verified through computer simulation. The ratio of the fundamental component of the Dicke ripple to the dc level at the output of the processor can then be determined to be

$$\rho = \frac{V_1}{V_o}$$
$$\rho = \frac{4}{\pi} \frac{(T_B + T_R)}{(T_B - T_R)} K_1 K_2 G(j\omega_d) \tag{2-27}$$

Substituting the appropriate value for the loop gain into equation (2-27) results in

$$\rho = \frac{8}{\pi} \frac{(308 + 627)}{(308 - T_A)} \left| \frac{31.195(1 + 2.545 \times 10^{-3} j\omega_d)}{j\omega_d(1 + 28 \times 10^{-3} j\omega_d)} \right| \times 100\%$$
$$\rho = \frac{3.658 \times 100\%}{308 - T_A} \tag{2-28}$$

This output peak ripple level expressed as a percentage of the output signal is shown as a function of antenna signal temperature in figure 2-6. From this curve, it is readily observed that the ripple level

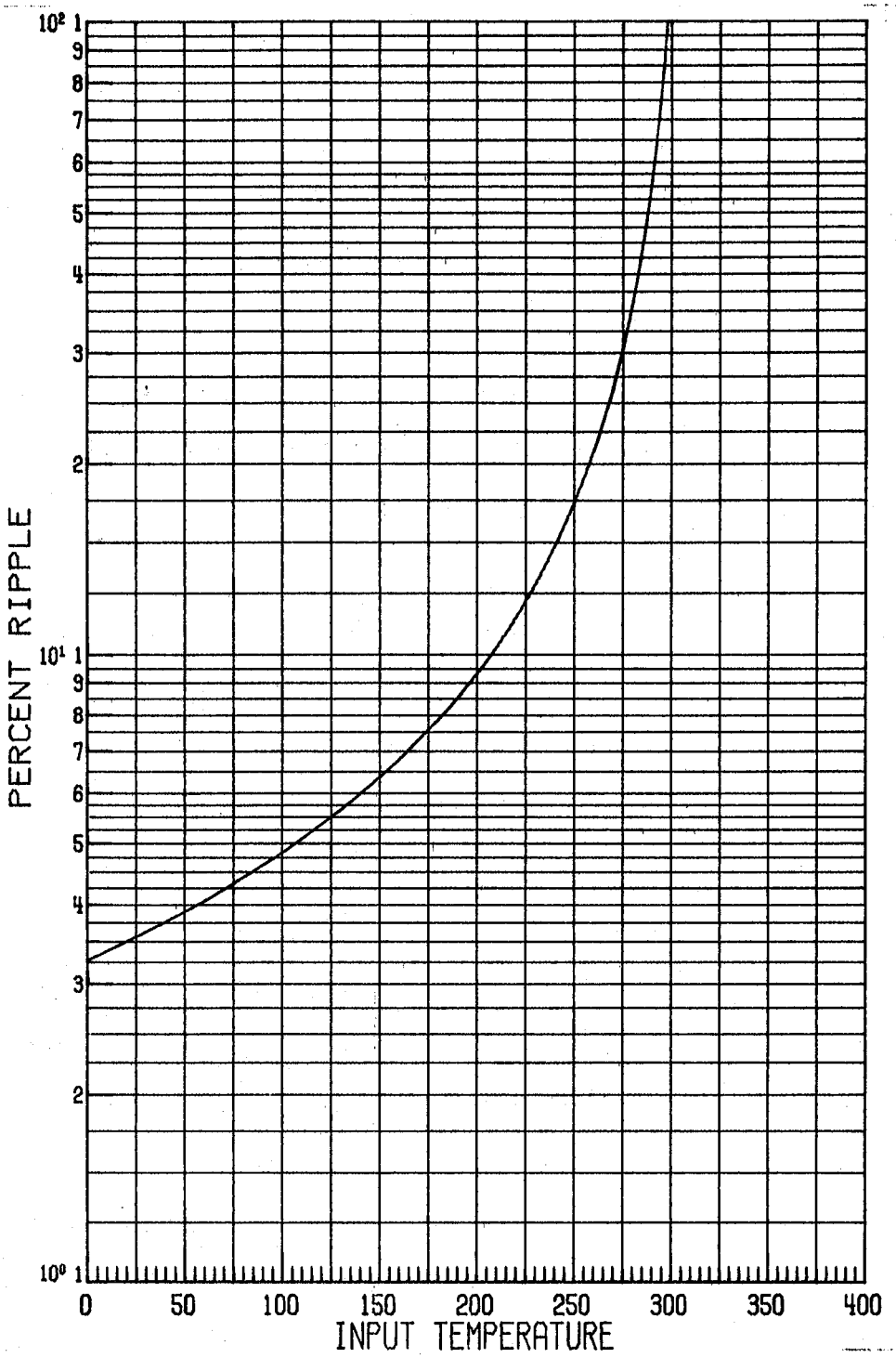

Figure 2-6. Ripple factor versus antenna temperature for present radiometer.

increases markedly with increasing input signal temperature and becomes quite significant for large antenna signal temperatures.

This Dicke ripple appears about the dc level at the output of the analog processor. Thus, as the ripple level increases the dynamic range available for the dc level decreases. This is undesirable since the dc level is the actual estimate of the received power. As the **ripple level increases the dynamic range required of the injection noise source increases. If the ripple becomes excessive the temperature range over which the radiometer can operate may be reduced.**

Through the use of the system model and the transfer function of equation (2-12), several aspects of the radiometer's performance were investigated above. The sensitivity of a radiometer was defined, and an expression for the sensitivity of this particular radiometer was obtained. The ripple associated with the Dicke switching process was calculated. The implications of time averaging a nonergodic process were examined. An expression for the bias error resulting from the use of a time average as an indicator of the ensemble average of a nonergodic process was developed. It was noted that this bias or "antenna smear" error became larger for longer averaging times, and that the bias error was a function of the actual brightness temperature to be measured. Thus, if the time average is to be used as an estimator of the actual brightness temperature, the optimum averaging or integration time will be a tradeoff between sensitivity and "antenna smear" error. It was determined that for a specified spatial resolution the optimum integration time is a function of the brightness temperature of the scene

being measured. Thus, the estimation scheme can be improved by performing measurements of several integration time and sensitivities. However, care must be taken since as the loop is made to respond faster to reduce the "antenna smear" error of a quickly changing scene, the Dicke ripple may increase, driving the radiometer into saturation. Thus, the power estimation strategy can be improved by reducing the Dicke ripple within the control loop and developing a variable integration time averaging scheme. In the following chapters a digital processing unit is designed, developed, and implemented which will improve the performance of the radiometer.

CHAPTER III

PROPOSED PROCESSING STRATEGY

In this chapter a power estimation strategy is developed which will improve the tradeoff between sensitivity and "antenna smear" error. It will be shown in this chapter that digital processing techniques can be used to improve the power estimate performance of the radiometer. Anomalies of the sample data approach will be exploited to reduce the Dicke ripple which will aid in the development of a variable integration time post-loop processing strategy. This post-loop strategy coupled with the added flexibility of the digital signal processor will result in an improved power estimation strategy.

A. Improved Processing Technique

When applying digital signal processing techniques to the radiometer, one of the first questions to be answered is at what point within the radiometer should the analog signal be sampled. Sampling as close to the antenna as possible seems desirable since a larger number of analog components will be replaced by the digital processor which is more stable and flexible. However, sampling prior to the square-law detector is not possible with presently available components since system bandwidths of 1 GHz or greater are required for proper radiometer operation. System bandwidth between the square-law detector and correlator should be maintained above 5 kHz for proper operation. However, after the square-law detector only the mean of the signal is of interest, and the question arises as to whether the signal can be undersampled without

undesirable effects. It has been shown, however, that although reconstruction of the signal in the conventional sense is not required, sampling below the Nyquist rate will cause a noise foldover effect [10]. This foldover effect is the conventional aliasing error, and it reduces the mean to variance power ratio. Therefore, if the signal is sampled before the correlator, a sample rate above 10 kHz would be required. It may be possible to develop the required digital processor with a data rate of 10 kHz, thus placing the aliasing filter and analog-to-digital (A/D) converter before the correlator. However, after the correlator, the signal could be filtered any amount since at this point any low-pass filtering provides additional smoothing in the estimate of the dc level of the signal. This fact coupled with some technical difficulties of a digital processor operating at 10 kHz result in the conclusion that sampling after the correlator is most desirable.

The selection of the sampling frequency should be made very carefully. Due to the periodic nature of the Dicke switch, the output of the correlator has line components at harmonics of the Dicke switch frequency. If the sampling frequency is selected as an odd harmonic of the Dicke switch frequency, the line components will be translated to dc by the sampling process causing a substantial error in the measurement of the actual dc level. However, due to the symmetry of the deterministic signal at the output of the correlator (with no injected noise), no line components exist at even harmonics of the switch frequency. Depending on the feedback method, the feedback noise pulses "riding" on this square wave may cause line components to be formed at these even harmonics.

Even so, sampling at an even harmonic of the Dicke switch frequency may still be very desirable.

Let us assume that an accumulator will exist within the microprocessor algorithm to replace the analog integrator. Consider the discrete transfer function $R(z)$ of the accumulator.

$$R(z) = \frac{1 + z^{-1}}{1 - z^{-1}} \tag{3-1}$$

The steady-state transfer function $R\left(e^{j\omega\tau_s}\right)$ is found to be

$$R\left(e^{j\omega\tau_s}\right) = \frac{1 + e^{-j\omega\tau_s}}{1 - e^{-j\omega\tau_s}}$$

$$= \frac{e^{\frac{j\omega\tau_s}{2}} + e^{\frac{-j\omega\tau_s}{2}}}{e^{\frac{j\omega\tau_s}{2}} - e^{\frac{-j\omega\tau_s}{2}}}$$

$$= -j \cot\left(\frac{\omega\tau_s}{2}\right) \tag{3-2}$$

where τ_s is the sample interval. The amplitude response $\left|R\left(e^{j\omega\tau_s}\right)\right|$ is shown in figure 3-1. This amplitude response approximates that of an ideal integrator for $f << 1/2\tau_s$. Note, however, that for $f = 1/2\tau_s$ the steady-state response is identically zero. That is, the accumulator has a transmission null at one-half the sampling frequency. Herein lies the motivation for selecting the sampling frequency as a harmonic of the Dicke switch frequency. If the sampling frequency is chosen as twice the Dicke switch frequency, the transmission nulls of the accumulator

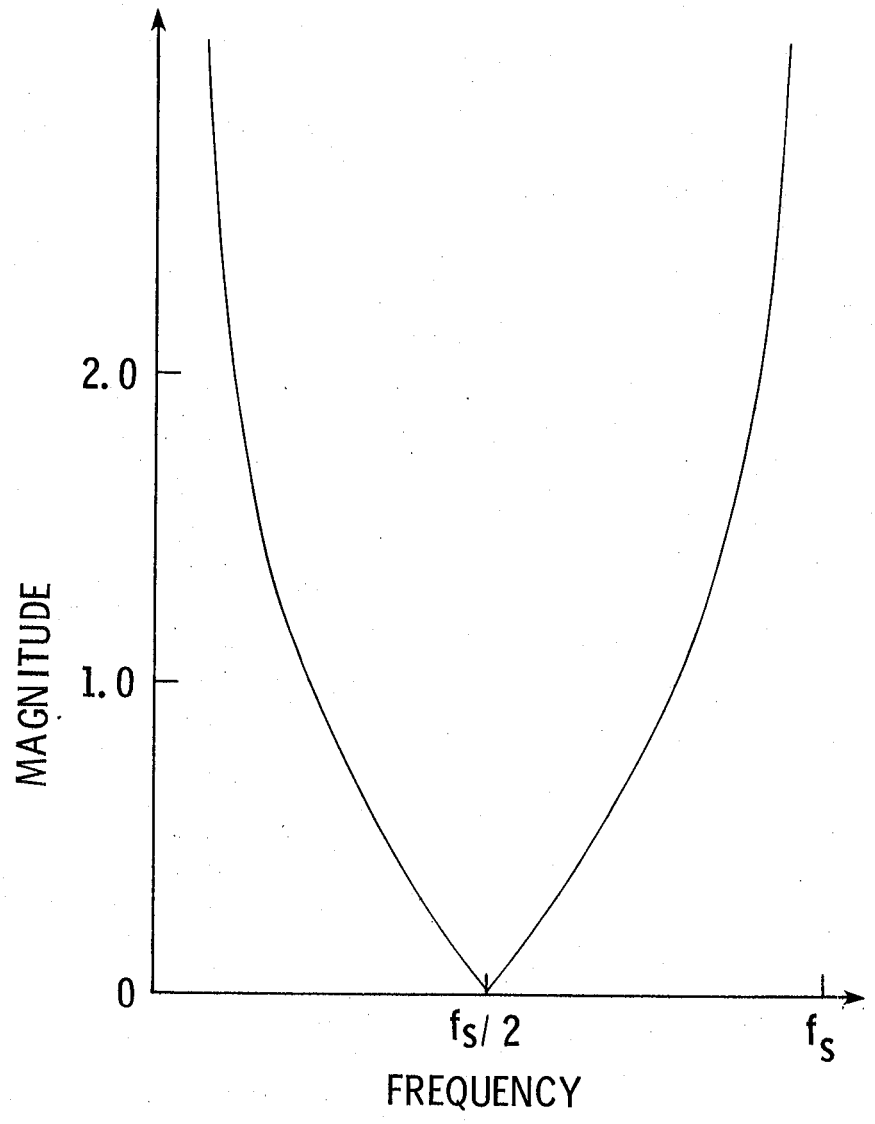

Figure 3-1. Magnitude response of accumulator algorithm.

will completely eliminate the line components at all odd harmonics of the Dicke switch frequency. Thus, all components of the Dicke ripple, except those introduced during the feedback process, have been eliminated. This should greatly reduce the undesirable Dicke ripple. It is also worth noting that if the sampling frequency is twice the Dicke frequency, the Dicke switch and analog-to-digital converter can easily be synchronized and can be controlled by the same clock.

If the sampling frequency is to be twice the Dicke frequency, an optimum Dicke frequency must be determined. The selection of the Dicke frequency is a compromise between ease of aliasing filtering and an excessive bandwidth requirement for amplifiers in the forward loop of the radiometer. A higher Dicke frequency provides more guard band between dc and harmonics of the switching frequency, thus easing aliasing filter requirements. However, a higher Dicke switch frequency also requires wider bandwidth amplifiers in the forward loop since these amplifiers should pass all significant components of the Dicke frequency. Through computer simulation, a Dicke switch frequency of 300 Hz proved to provide acceptable aliasing filter requirements and did not require excessive bandwidths of the forward loop amplifiers. If the Dicke switch frequency is chosen as 300 Hz, the sampling frequency should be chosen as 600 Hz. The accumulator then eliminates odd harmonics of the Dicke switch frequency, thus reducing the Dicke ripple effect.

The aliasing filter is selected to minimize the aliasing or noise foldover problem discussed earlier without substantially affecting the control loop; i.e., the closed-loop response should be exclusively

determined by the digital processor algorithm. With the selected sampling frequency of 600 Hz, the aliasing filter should attenuate the spectrum above 300 Hz to minimize noise foldover. The only portion of the signal that is of interest at this point is dc, so the flatness of the passband is not of interest. A simple low-pass filter having three real poles at 100 Hz was found to meet these requirements. At 300 Hz, this network attenuates the spectrum 30 dB and rolls off at a rate of 60 dB/decade. Computer simulations indicated that this network reduced the noise foldover to insignificant levels, and the effect of this aliasing filter on the closed-loop response was found to be minimal.

It was noted earlier that line components in the correlator output may be formed at even harmonics of the Dicke switch frequency due to the feedback pulses. If such line components were formed, they would be translated directly to dc when sampled at 600 Hz and would cause significant error. Simulations proved that all these even harmonic components except the one at 600 Hz were attenuated sufficiently to cause negligible error. The component at 600 Hz is attenuated 47 dB by the aliasing filter. However, when sampled, it is translated to dc and causes an error in the measurement. To eliminate this error, a notch filter with a null at 600 Hz is added to the aliasing filter.

The sampled output of the aliasing filter is operated on by the microprocessor algorithm. The algorithm must form an estimate of the mean of the input signal. Just as for the analog processor, the problem of finding an integration time for minimum error arises. As discussed in Chapter II, a slower control loop, i.e., increased integration time,

will reduce fluctuation error, but will increase the "antenna smear" error or reduce spatial resolution. The digital processor, however, can adjust the loop time constant under program control. Thus, an operator, or possibly the microprocessor, itself, could estimate the "antenna smear" error given in equation (2-15) and appropriately adjust the integration time to minimize total error for a specified spatial resolution. To provide this flexibility, the algorithm must estimate the mean of the input over several integration times. There are two obvious methods which would provide this capability. First, the loop filter could be adjusted under program control, thus modifying the loop response. The second method would be to design a first order loop with a settling time equal to the shortest integration time required. Post-loop averaging can then be performed on the loop output to reduce estimate variance. It was decided that the second method would be most desirable since the first order loop has certain design advantages, and the estimates for all accuracies are available simultaneously.

In order to form the required first order loop, the loop filter contained in the analog process is eliminated from the microprocessor algorithm, and the analog integrator is replaced by an accumulator. As mentioned earlier, the accumulator has the desirable effect of eliminating the odd harmonics of the Dicke ripple. The output of the accumulator will control the feedback noise, thus completing the loop. It was determined that an integration time of 100 ms was the minimum value required. A first order loop with a damping factor of 50 will provide this minimum integration time. The loop gain required to obtain a

damping factor of 50 will be calculated in the next chapter. To provide the longer integration times, the output of the loop is further averaged by a post-loop processor.

The post-loop processor sums N loop samples and then divides by N. To simplify the algorithm, N is restricted to integer powers of two. To limit the dynamic range required and avoid the possible need for floating point arithmetic, a partitioning averaging scheme will be implemented. In this averaging scheme, which is actually several sum-and-dump algorithms, two samples out of the loop are added together and then divided by two. This output will be denoted as $y_2(n)$, where n is the post-loop sampling integer. Then $y_2(n)$ is added to the previous value, i.e., $y_2(n-2)$, and divided by two resulting in $y_4(n)$. Let $y_1(n)$ represent discrete values appearing at the output of the loop. The remaining values out of the post-loop processor can be expressed as

$$y_2(n) = \frac{y_1(n) + y_1(n-1)}{2} \tag{3-3}$$

$$y_4(n) = \frac{y_1(n) + y_1(n-1) + y_1(n-2) + y_1(n-3)}{4}$$

$$y_4(n) = \frac{y_2(n) + y_2(n-2)}{2} \tag{3-4}$$

$$y_8(n) = \frac{1}{8} \sum_{i=0}^{7} y_1(n-i)$$

$$y_8(n) = \frac{y_4(n) + y_4(n-4)}{2} \tag{3-5}$$

$$y_{16}(n) = \frac{1}{16}\sum_{i=0}^{15} y_1(n-i)$$
$$y_{16}(n) = \frac{y_8(n) + y_8(n-8)}{2} \qquad (3\text{-}6)$$

$$y_{32}(n) = \frac{1}{32}\sum_{i=0}^{31} y_1(n-i)$$
$$y_{32}(n) = \frac{y_{16}(n) + y_{16}(n-16)}{2} \qquad (3\text{-}7)$$

$$y_{64}(n) = \frac{1}{64}\sum_{i=0}^{63} y_1(n-i)$$
$$y_{64}(n) = \frac{y_{32}(n) + y_{32}(n-32)}{2} \qquad (3\text{-}8)$$

The partitioning averaging scheme uses the previously averaged output to form the next averaged output. This partitioning scheme, in addition to reducing dynamic range requirements, uses far less memory and processor time than the direct averaging method.

The post-loop averaging should decrease the ΔT of the loop output. To determine how well the sum-and-dump algorithm decreases the fluctuations of the measurement, the effect of this algorithm on the variance of the loop output should be studied. It will be assumed that the input to the post-loop processor is ergodic and stationary (negligible "antenna smear" error). The variance of the $y_N(n)$ output of the post-loop processor is then determined to be

$$\sigma^2_{y_N} = \text{Var}\left\{ y_N(n) \right\} = \text{Var}\left\{ \frac{1}{N} \sum_{i=0}^{n-1} y_1(n - i) \right\} \tag{3-9}$$

It can be shown that if the samples $y_1(n - i)$ are statistically independent, equation (3-9) can be written as

$$\sigma^2_{y_N} = \frac{\sigma_y^2}{N} \tag{3-10}$$

Thus, if the samples at the loop output are statistically independent, the sum-and-dump averaging reduces the variance of the output fluctuations by $1/N$.

In addition to providing data for the post-loop processor, the output of the first order loop must control the duty cycle of the injected noise pulses, thus controlling the feedback noise. Due to the sensitivity of the steady-state error of the radiometer to variations in the feedback path, it is desired to keep the feedback path within the processor algorithm as much as possible. The feedback will be accomplished by loading the N bit word out of the loop into a down counter and clocking the down counter at a rate of $2^N - 1$ times the sample rate. The injected noise is on when the down counter contains a word greater than zero and is cutoff when the down counter reaches zero. In this way, the level of the injected noise power is adjusted to any of 2^N levels. It is also desired to improve the injection scheme by injecting the noise in the early portion of the Dicke cycle to reduce the loss of the injected pulse due to rounding of the pulses as discussed in Chapter II. If the down counter is started at the beginning

of the antenna portion of the Dicke cycle, and if the maximum duty cycle is kept somewhat less than 100 percent, the injected noise loss due to rounding and spillover can be virtually eliminated.

The maximum duty cycle or maximum injected noise corresponds to the minimum input temperature. Referring to the feedback path of figure 2-2, based on a reference source of 308 K, a directional coupler coefficient of -20 dB, an excess noise diode temperature of 365,000 K, and the original 6 dB fixed attenuator, the maximum duty cycle is

$$d_{max} = \left[\frac{308}{0.01} - 308\right] \Big/ \left[(365{,}000)(0.25)\right] = 0.334 \qquad (3\text{-}11)$$

In order to increase the length of a typical noise pulse and reduce quantization error in the feedback, the maximum duty cycle is increased to near unity. To increase the duty cycle, the fixed attenuator was changed to 10 dB, and the maximum duty cycle then becomes

$$d_{max} = \left[\frac{308}{0.01} - 308\right] \Big/ \left[(365{,}000)(0.10)\right] = 0.835 \qquad (3\text{-}12)$$

This noise injection scheme differs considerably from the original design in that it will be injecting noise continuously during a portion of the Dicke cycle. The injection scheme provides excellent feedback stability, and with a maximum duty cycle of 0.835 will virtually eliminate the noise spillover into the reference half cycle. However, it does introduce a slight error due to the finite bandwidth of the video amplifier. The video amplifier has a bandwidth of 5 kHz and will reject the portion of the input spectrum above 5 kHz. Since narrower pulses will have a

wider frequency spectrum than wider pulses, the video amplifier will reject a larger proportion of power for narrow pulses than for wide pulses. This slight error can be compensated for by careful calibration and subsequent adjustment of recorded data.

In summary, the proposed digital signal processor should filter the output of the correlator with three simple one pole sections, each with a cutoff frequency of 100 Hz, and a notch at 600 Hz. The output of this aliasing filter is sampled at 600 Hz, and the samples are processed by the digital filter algorithm. The output of the digital filter algorithm is used to control the feedback pulses and is further processed by the post-loop processing algorithm. A block diagram of this proposed system is shown in figure 3-2.

B. Implementation

The hardware required to implement this proposed digital processor can be considered as being composed of four sections: an aliasing filter, an analog-to-digital converter, the microprocessor for implementation of the algorithm, and a section to generate the timing signals required by the radiometer and to control the feedback.

The aliasing filter is composed of the three low-pass sections and the notch filter. The three real poles of the aliasing filter are provided by the circuit shown in figure 3-3. The transfer function of this circuit can be shown to be

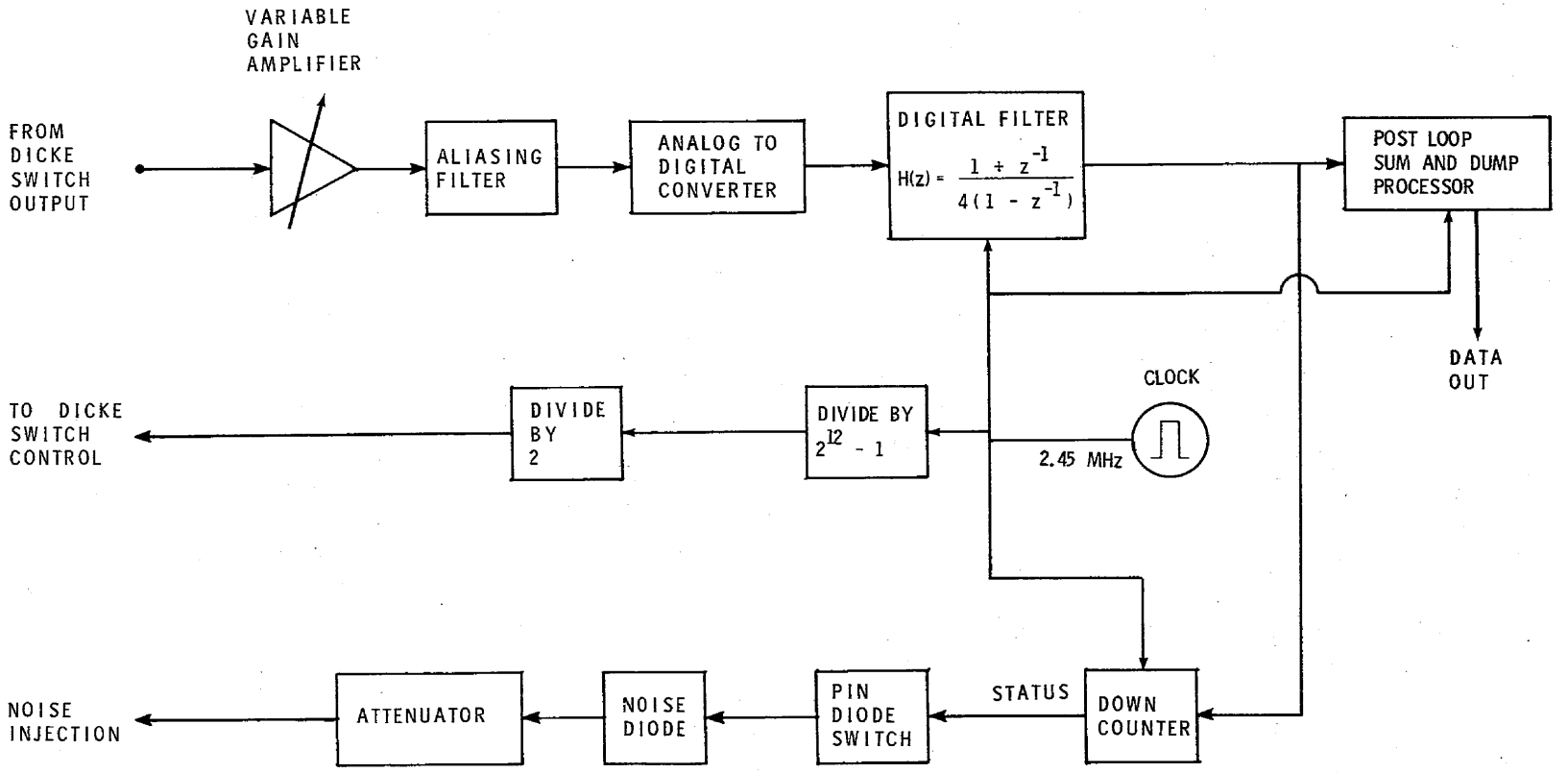

Figure 3-2. Proposed digital signal processor.

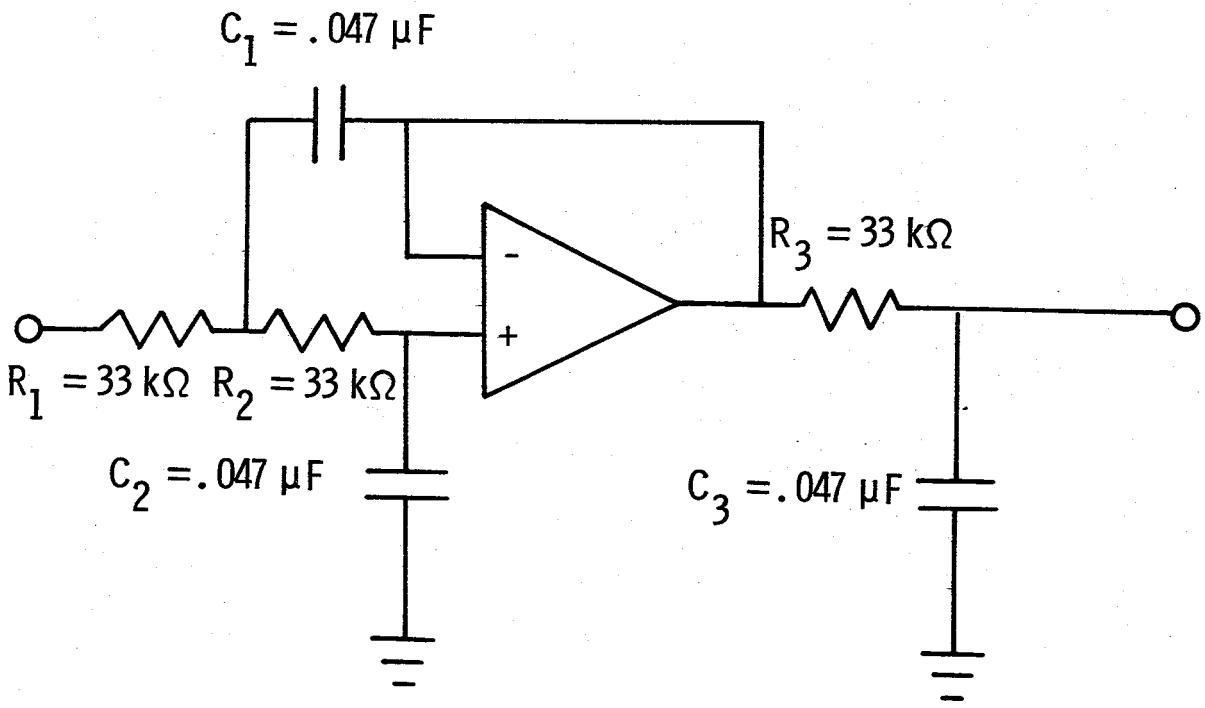

Figure 3-3. Three pole filter.

$$G_{F_1}(s) = \frac{\dfrac{K_2}{R_1C_1R_2C_2R_3C_3}}{\left[s^2 + s\left(\dfrac{1}{R_1C_1} + \dfrac{1}{R_2C_2}\right) + \dfrac{1}{R_1C_1R_2C_2}\right]\left(s + \dfrac{1}{R_3C_3}\right)} \qquad (3\text{-}13)$$

For the component values shown in figure 3-3, equation (3-13) becomes

$$G_{F_1}(s) = \frac{(200\pi)^3}{\left[s^2 + s(800\pi) + (200\pi)^2\right]\left[s + (200\pi)\right]} \qquad (3\text{-}14)$$

$$G_{F_1}(s) = \frac{1}{\left(1 + \dfrac{s}{200\pi}\right)^3}$$

From equation (3-14), the circuit of figure 3-3 clearly provides the required three real poles. The notch at 600 Hz is developed using the circuit illustrated in figure 3-4. The transfer function associated with figure 3-4 can be shown to be

$$G_{F_2}(s) = \frac{s^2 + (1200\pi)^2}{s^2 + s(4800\pi) + (1200\pi)^2} \qquad (3\text{-}15)$$

Combining the three pole and notch filters of figures 3-3 and 3-4 results in the required aliasing filter shown in figure 3-5, where IC2 is inserted to isolate R_3C_3 from the notch filter. When equations (3-14) and (3-15) are combined the transfer function $G(s)$ of the aliasing filter (shown in figure 3-5) is

$$G(s) = \frac{\left[s^2 + (1200\pi)^2\right](200\pi)^3}{\left[s^2 + s(4800\pi) + (1200\pi)^2\right](s + 200\pi)^3} \qquad (3\text{-}16)$$

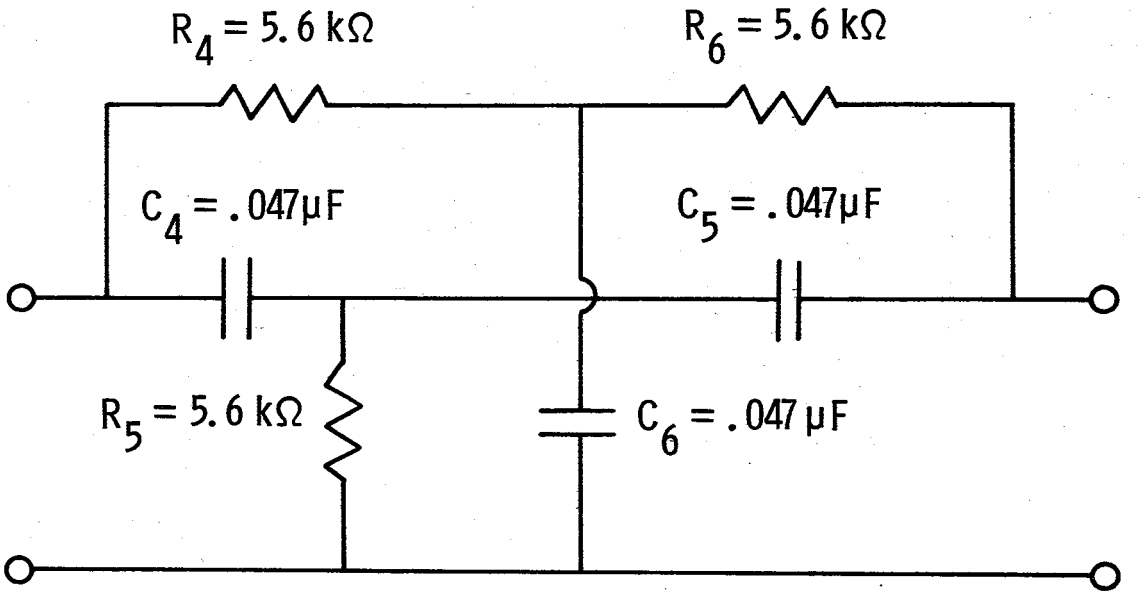

Figure 3-4. Notch filter.

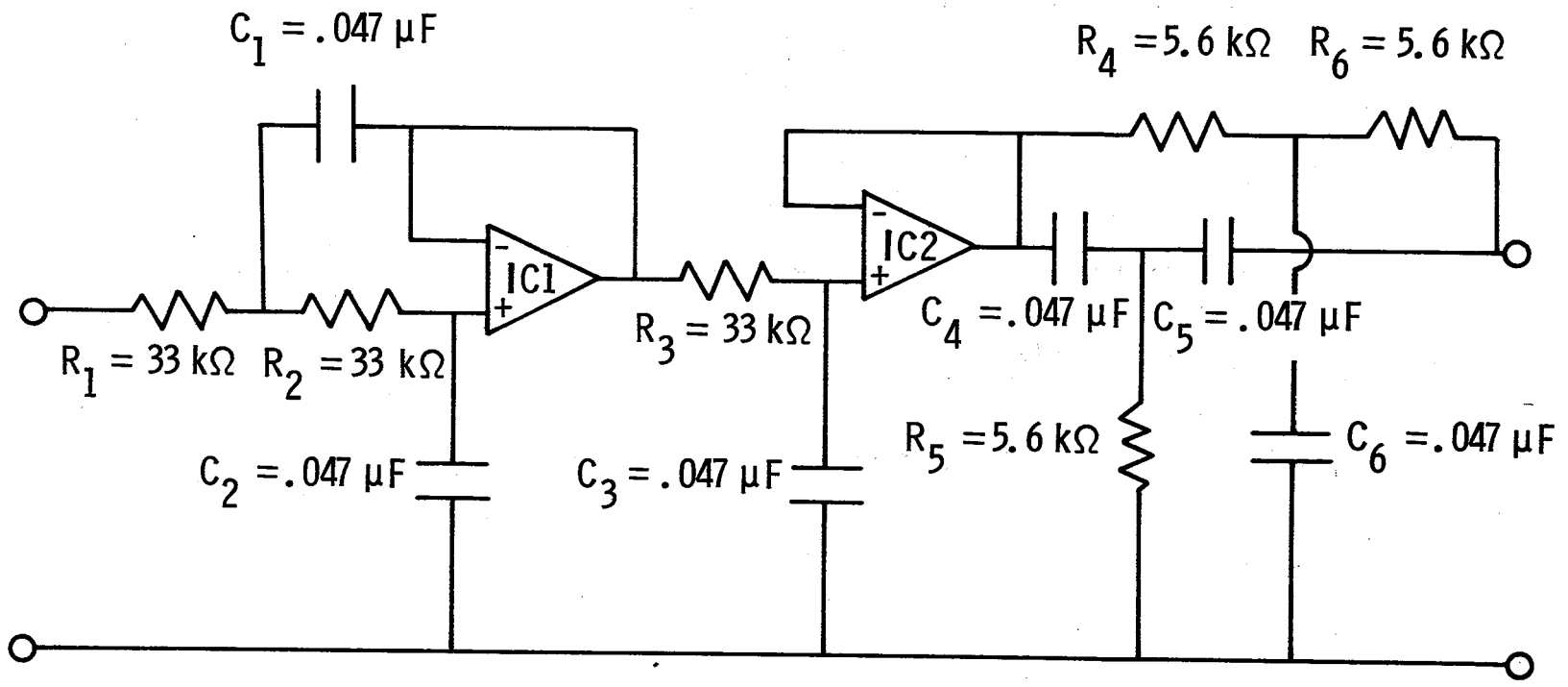

Figure 3-5. Required aliasing filter.

The aliasing filter requirement specified earlier in this chapter is met by equation (3-16). Thus, the network shown in figure 3-5 is an adequate aliasing filter.

The output of this filter must now be sampled by the analog-to-digital converter. The first aspect of this analog-to-digital converter to be considered is that resolution uncertainties should be significantly less than the fluctuations inherent in the measurement. Using equation (2-16) and the equivalent output noise bandwidth of the loop given in equation (4-8), the fluctuation of the output of the loop is given by

$$\Delta T = 1870 \sqrt{\frac{25}{B_{SI}}} \tag{3-17}$$

where B_{SI} is the input statistical bandwidth. Substituting the appropriate values for B_{SI} the fluctuation ΔT at the output of the loop ranges from 2.1 K to 0.21 K corresponding to a range of B_{SI} from 20 MHz to 2 GHz. The minimum input temperature of interest is 100 K; therefore, the fluctuations in the measurement at the loop output range from 2.1% to 0.21% of the values to be measured. The resolution of an N bit analog to digital in a bipolar offset format is given by

$$r = \pm 2^{-N} \times 100\% \tag{3-18}$$

Due to the fluctuations inherent in the measurement process as well as uncertainties in the radiometer exterior to the signal processing section, a resolution of approximately 10% of the minimum ΔT (i.e., 0.02%) was determined to be tolerable. Using equation (3-18), the

number of bits required for this resolution was determined to be 12.1. This value is so close to 12, it was determined that 12 bits would be sufficient. The Analog Device's AD572 was selected as the analog-to-digital converter since, in addition to its 12 bit resolution, it is extremely linear and has a fast conversion time (25 μs).

In order to obtain an accuracy within one-half of the least significant bit (±1/2 LSB) from the AD572, the input signal must not change by more than 1/2 LSB during the conversion time. The maximum amount by which the input can change during the conversion interval is given by

$$\Delta V = \frac{V_R}{2^{N+1}} \tag{3-19}$$

where V_R is the input range of the analog-to-digital converter. If the range of the AD572 is adjusted to ±2.5 V (V_R = 5 V) then since the AD572 is a 12 bit converter ΔV is determined to be

$$\Delta V = \frac{5\ V}{2^{13}}$$

$$= 0.61\ mV \tag{3-20}$$

Since the conversion time of the AD572 is approximately 25 μs, the maximum allowable rate of change of the input voltage is

$$\left.\frac{\Delta V}{\Delta t}\right|_{max} = \frac{0.61\ mV}{25\ \mu s}$$

$$= 24.4\ V/s \tag{3-21}$$

A more meaningful result may be obtained by computing the maximum frequency of a ±2.5 volt sine wave which does not exceed the maximum rate of change. The maximum rate of change of a sine wave occurs as it goes through zero and is equal to

$$\left.\frac{dV}{dt}\right|_{max} = (V_p)(2\pi f) \tag{3-22}$$

where V_p is the peak level of the sine wave. Solving for frequency in equation (3-22), and substituting 2.5 for V_p, the result is

$$\begin{aligned} f_{max} &= \frac{1}{5\pi}\left.\frac{dV}{dt}\right|_{max} \\ &= \frac{1}{5\pi}(24.4) \\ &= 1.55 \text{ Hz.} \end{aligned} \tag{3-23}$$

Since the aliasing filter has a cutoff frequency well above 1.55 Hz, a sample-and-hold device must be included in the design.

The requirements on the microprocessor are not very stringent since care was taken in developing the digital algorithm to minimize the arithmetic operations which the microprocessor would have to perform. The microprocessor must implement the accumulator and post-loop algorithms, and it will operate in fixed point arithmetic. The microprocessor will interpret the binary point as leading all bits, i.e., the maximum value is $1-2^{(-N+1)}$. There is a 4 to 1 expansion (two bits) through the accumulator, and the microprocessor must operate on 14 bit words to accommodate this expansion. Many microprocessors are available

which could easily fulfill these requirements with a data rate of 600 Hz. An Intel 8086 microprocessor was used in the prototype design solely due to availability. The 8086 is a 16 bit microprocessor and so can easily operate on the required 14 bit words. However, with the relatively slow sample rate and simple algorithm, an 8 bit microprocessor operating with double precision could also implement the algorithm.

To reduce the possibility of an overflow due to the expansion in the accumulator, the samples out of the analog-to-digital converter are sign extended and loaded into the 12 least significant bits of the microprocessor. Since the 8086 has 16 bit words, the maximum input voltage of 2.5 V will be interpreted by the microprocessor as $2^{-4} - 2^{-15}$. Thus, there is a "redefinition" gain of

$$K_{ADC} = (2^{-4} - 2^{-15})/2.5$$
$$K_{ADC} \approx 0.025 \qquad (3\text{-}24)$$

The output of the accumulator will be a 14 bit word located in the 14 least significant bits. In order to have available the most significant 12 bits, the output word is shifted right 2 bits which is equivalent to the divide by 4 shown in figure 3-2. When these 12 bits are sent to the down counter, it will interpret all 12 bits being "one" as the level $1-2^{-16}$. Thus there is another "redefinition" gain of 16. The control loop model including "redefinition" gains is shown in figure 3-6. A flow chart of the required algorithm is shown in figure 3-7. The

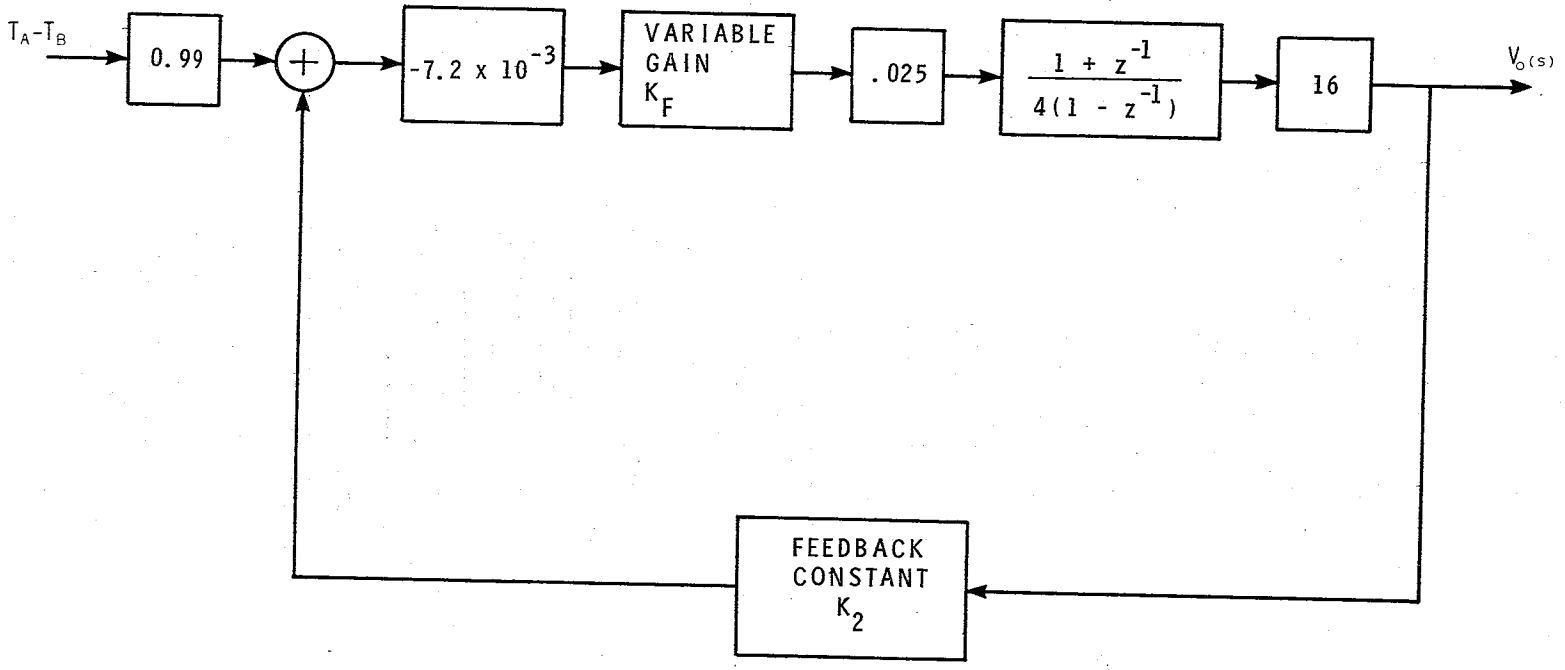

Figure 3-6. Control model of proposed digital processing radiometer.

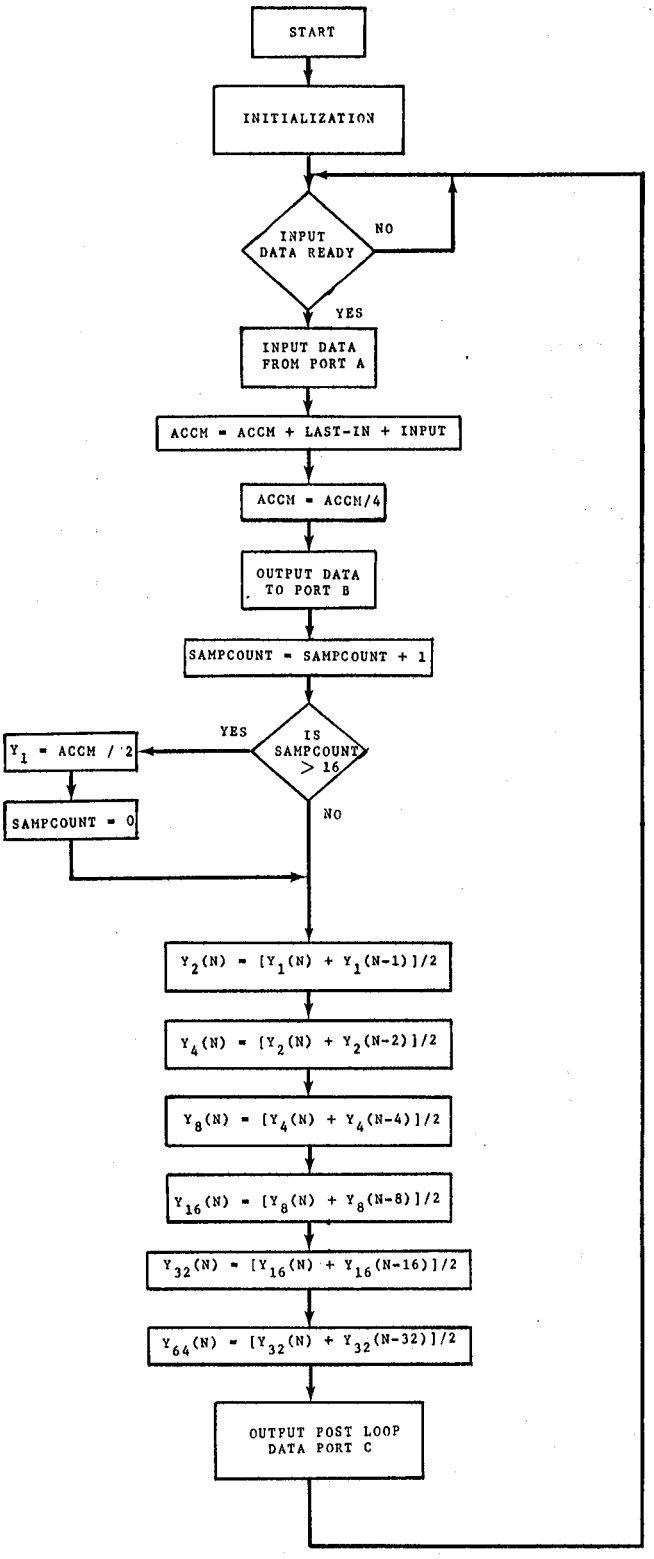

Figure 3-7. Processor algorithm flow chart.

algorithm consists of two adds and two right shifts for the accumulator and six adds and right shifts for the post-loop processor, in a minimum of 14 bit arithmetic. The microprocessor must also have available enough Read Only Memory (ROM) to store the required instruction code and six 14 bit words of Random Access Memory (RAM) to store the previous values of the post-loop outputs.

The digital processor must also generate the Dicke switch drive and the control pulse for the noise diode. These timing signals are obtained through the use of the Intel 8253 Programmable Interval Timer. The 8253 consists of three independently programmable 16 bit counters. Each counter can be programmed to operate in any of six modes. Counter 0 of the 8253 will be programmed as a divide by N counter. In this mode, the output of counter 0 will stay high for N clock cycles, then go low for one clock cycle, and return high for another N cycles. This counter will be used to divide the 2.45 MHz microprocessor clock by $2^{12} - 1$. The output of this counter will be a 598.29 Hz pulse train used to control the analog-to-digital converter. Counter 1 will be programmed as a variable monostable multivibrator (commonly referred to as a one-shot). In the one-shot mode, the output of counter 1 will go low when the gate 1 input goes high and stays low for N clock cycles, where N is the digital word loaded into the counter. The output of the loop algorithm will be loaded into counter 1. It is then triggered at the beginning of the Dicke cycle. Thus, the duty cycle of the output of counter 1 is controlled by the output word from the accumulator algorithm. The third

counter is also programmed as a one-shot and it is used to complete the "handshaking" between the analog-to-digital converter and the microprocessor.

Combining the filter, analog-to-digital counter, and the 8253, the digital signal processor shown in figure 3-8 is formed. The output of counter 0 is inverted and used as the start convert pulse. The output of counter 0 is also used to clock the D-type flip-flop of the 7474 which converts the pulse train into a square wave of one-half the pulse train frequency. The square wave output of the flip-flop is used as the Dicke switch drive. As the analog-to-digital converter receives the start convert pulse and begins the conversion, the status line goes high. This status line enables the sample and hold circuit which holds the signal at the input to the analog-to-digital converter constant for the entire conversion interval. At the end of the conversion, the status line goes low which triggers the one-shot of counter 2 of the 8253. The output of counter 2 goes low directing the microprocessor to service the input port. The output of the loop algorithm is loaded into counter 1 of the 8253, which is programmed as a variable one-shot. Counter 1 is triggered by the Dicke drive such that the output goes low at the beginning of the antenna portion of the Dicke cycle and stays low until the counter content reaches zero. The output of counter 1 is used to control the noise diode, i.e., the injected noise. Note that all required timing is derived from the microprocessor clock (see figure 3-8). Thus, variations of the clock frequency do not disturb the operation of the radiometer.

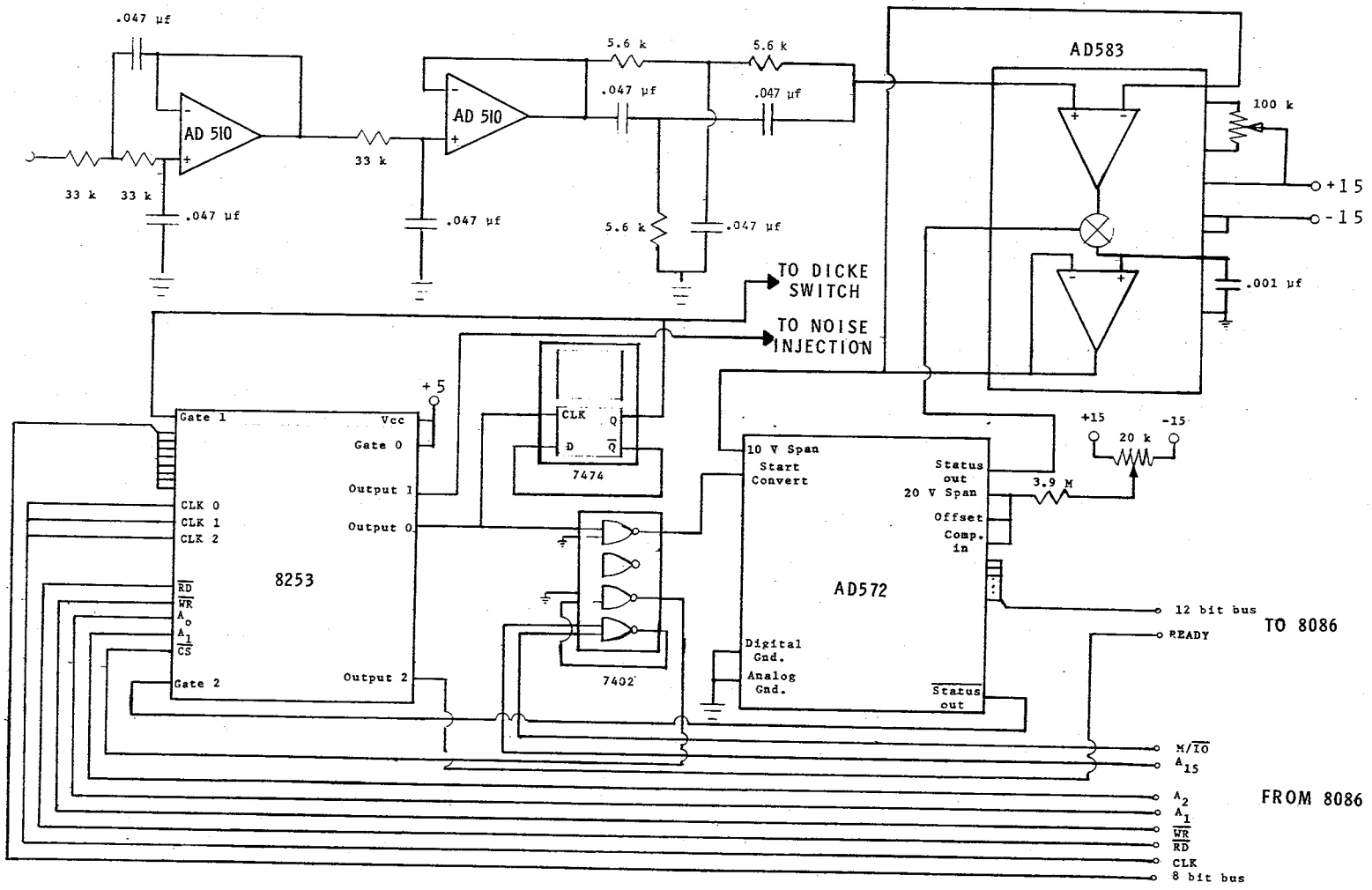

Figure 3-8. Digital signal processor circuit diagram.

The digital processor illustrated in figure 3-8 has been developed with the idea of exploiting advantages of the digital process in mind. This processor should substantially reduce the Dicke ripple within the control loop, thus making possible integration times much shorter than were obtainable with the original design. The shorter integration times allow most of the averaging to be done in the more efficient post-loop algorithm. The flexibility of the digital processor and the use of the post-loop processing strategy produce simultaneous estimates of several integration times. This flexible averaging scheme allows an operator, or possibly the microprocessor itself, to select the integration time resulting in the best estimate for a specified spatial resolution. Results of an analysis of this new estimation strategy and experimental results obtained using the prototype discussed in this chapter are presented in the next chapter to verify the improved estimation performance of the radiometer.

CHAPTER IV

RESULTS

An analysis of the proposed estimation strategy and the corresponding analytical results are presented in the first section of this chapter. In the second section experimental results will be presented.

A. Analytical

In order to determine a model for the first order control loop, the discrete time transfer function of the accumulator given by

$$R(z) = \frac{1 + z^{-1}}{1 - z^{-1}} \tag{4-1}$$

where z represents the Z-transform variable, must be transformed to its continuous time approximation. The direct relationship between the s-plane and the z-plane is given by

$$z = e^{s\tau_s} \tag{4-2}$$

where τ_s is the sample interval.

Then by use of the Taylor expansion, equation (4-1) can be approximated at low frequencies as

$$R'(s) = \frac{2}{\tau_s s} \tag{4-3}$$

For the selected sampling rate of approximately 600 Hz, equation (4-3) becomes

$$R'(s) = \frac{1200}{s} \tag{4-4}$$

Referring to figure 3-6 and using the same values for the gain of the RF subsystems, since R'(s) is the dominant pole in the loop response, the forward loop transfer function is

$$G(s) = \frac{(2.88 \times 10^{-3})(1200)(K_F)(0.4)(1/4)}{s} \qquad (4\text{-}5)$$

where K_F is an adjustable gain in the forward loop. The feedback constant K_2 can be determined by considering how much noise is fed back for an output digital word of all "ones." When all "ones" appear at the output, the equivalent decimal value is interpreted to be $1\text{-}2^{-16}$. The binary point is interpreted as leading all bits. When the output word contains all "ones," the noise diode remains on for the entire half of the Dicke cycle, and the feedback noise is equivalent to 365 K. Thus, the feedback constant is $K_2 = 365$. The closed-loop response of the preposed digital processor as part of the radiometer can now be determined as

$$H_{CL}(s) = \frac{\dfrac{K_F(1200)(2.88 \times 10^{-3})(0.4)(1/4)}{s}}{1 + \dfrac{K_F(1200)(2.88 \times 10^{-3})(365)(0.4)(1/4)}{s}}$$

$$H_{CL}(s) = \frac{\dfrac{1}{365}}{1 + \dfrac{s}{126.14\ K_F}} \qquad (4\text{-}6)$$

It was determined that a damping factor of 50 is required. Clearly, if a damping factor of 50 is desired, then K_F should be 0.396, and (4-6) becomes

$$H_{CL}(s) = \frac{\frac{1}{365}}{1 + \frac{s}{50}} \tag{4-7}$$

The output of this loop is transferred to the post-loop processor. The post-loop processor then further averages the samples from the loop, and if the samples are statistically independent, it reduces the variance of the mean of the samples by 1/N. However, as the samples in the post-loop processor become statistically dependent, they provide less additional information about the process, and the variance of the estimate is reduced by less than 1/N.

To determine if the samples out of the loop are statistically dependent, the noise bandwidth of the loop should be found. The equivalent noise bandwidth of the output of the first order loop is calculated as

$$\begin{aligned} B_{NL} &= \frac{1}{G_{CL}^2(o)} \int_0^\infty |G_{CL}(f)|^2 \, df \\ &= \int_0^\infty \frac{df}{1 + \left(\frac{2\pi f}{50}\right)^2} \\ &= \frac{50}{2\pi}\left[\tan^{-1}\left(\frac{2\pi f}{50}\right)\right]_0^\infty \\ &= \frac{50}{2\pi}\left[\frac{\pi}{2} - 0\right] \\ &= \frac{50}{4} \\ &= 12.5 \text{ Hz} \end{aligned} \tag{4-8}$$

Since the output equivalent noise bandwidth of the closed-loop response is 12.5 Hz, samples closer together than approximately $1/(2B_{NL})$ or 40 ms apart will display a degree of correlation. The loop operates at 600 Hz so samples are available at the output of the loop every 1.66 ms. Clearly, these samples would be highly correlated. Since the efficiency of the post-loop process decreases as the samples become correlated, it would be more efficient for the post-loop processor to sample the output of the loop such that it only operates on uncorrelated samples. Of interest here is the optimum reduction in variance in a specific averaging time. Thus, as the sample rate is reduced to insure uncorrelated samples, care must be taken not to reduce the number of available uncorrelated samples such that the variance of the sample set is increased.

When attempting to sample the output of the loop, the sample rate should be chosen to provide the maximum number of uncorrelated samples available from the loop output in the specified time. Oversampling, that is, taking samples too close together, will provide the best possible reduction in variance for the averaging time. However, this is not optimum since the same reduction in variance could have been obtained using fewer samples. Undersampling, that is, taking samples so far apart that fewer than the available uncorrelated samples are taken, will increase the variance of the sample set. Thus, although the samples are uncorrelated the increased variance of the sample set results in less than optimum reduction in the variance for the specified averaging time. It was decided that if the loop output were sampled at 37.5 Hz or every 16th sample out of the loop all available uncorrelated samples

would be obtained. However, at this sample rate (26.66 ms) the output will be oversampled and so the samples into the post-loop processor will be somewhat correlated.

A model must now be developed describing the effect of the post-loop processor on samples which are not statistically independent. In the earlier description of the post-loop processor, the assumption was made that the samples were statistically independent. With this assumption the post-loop processor was found to reduce the variance of the samples by 1/N. If this assumption is not made, the purely statistical approach of equation (3-10) to modeling the post-loop processor becomes unwieldy, and the results obtained provide little insight into the process.

An analysis of the post-loop processor from a frequency domain viewpoint will provide an adequate model of the post-loop processor. The post-loop processor is illustrated from the z-transform point of view in figure 4-1. Consider the form of the post-loop algorithm

$$y_N(n) = \frac{1}{N} \sum_{i=0}^{N-1} y_1(n - i) \tag{4-9}$$

where $y_N(n)$ is the N averaged post-loop output and $y_1(n)$ is the loop output. Let $Y_N(z)$ represent the z-transform of $y_N(n)$, and let $Y_1(z)$ represent the z-transform of $y_1(n)$. Transformation of both sides of equation (4-9) yields

$$Y_N(z) = \frac{1}{N} \sum_{i=0}^{N-1} z^{-i} Y_1(z) \tag{4-10}$$

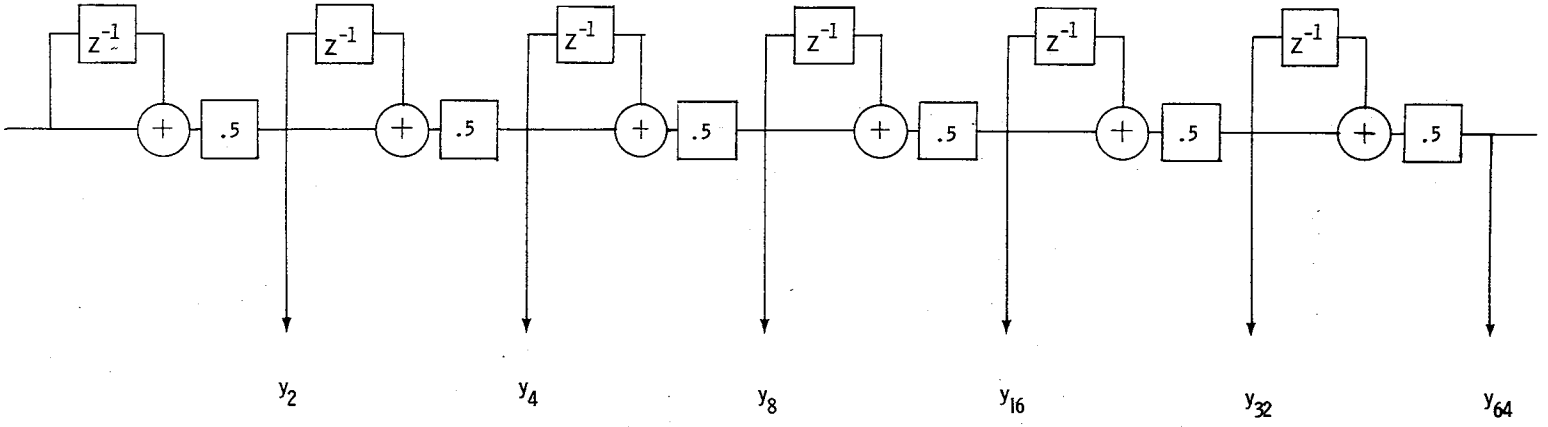

Figure 4-1. Sum and dump algorithm z-transform representation.

The transfer function of the post-loop processor can be expressed as

$$P(z) = \frac{Y_N(z)}{Y_1(z)} = \frac{1}{N} \sum_{i=1}^{N-1} z^{-i} \tag{4-11}$$

The steady-state frequency response can be found by substituting $z = e^{j\omega\tau_o}$ into equation (4-11)

$$P(j\omega) = \frac{1}{N} \sum_{i=1}^{N-1} e^{-j\omega\tau_o i} \tag{4-12}$$

where τ_o is the post-loop sample time, which is equal to sixteen times the loop sample interval; i.e., $\tau_o = 16\,\tau_s$. With the aid of the summation formula

$$\sum_{i=0}^{N-1} a^i = \frac{1 - a^N}{1 - a} \tag{4-13}$$

equation (4-12) can be written as

$$P(j\omega) = \frac{1 - e^{j\omega\tau_o N}}{N(1 - e^{j\omega\tau_o})}$$

$$P(f) = \frac{1 - e^{j2\pi f\tau_o N}}{N(1 - e^{j2\pi f\tau_o})} \tag{4-14}$$

$$P(f) = \frac{(e^{-j\pi f\tau_o N} - e^{j\pi f\tau_o N})e^{+j\pi f\tau_o N}}{N(e^{-j\pi f\tau_o} - e^{j\pi f\tau_o})e^{+j\pi f\tau_o}}$$

$$P(f) = \frac{\sin(\pi N\tau_o f)}{N \sin(\pi\tau_o F)}\, e^{+j(N-1)\pi f\tau_o}$$

The equivalent one-sided noise bandwidth of the post-loop processor is given by

$$B_{NP} = \left[\frac{1}{P(o)}\right]^2 \int_0^{1/2\tau_o} |P(f)|^2 \, df$$

$$= \int_0^{1/2\tau_o} \left[\frac{\sin(\pi N\tau_o f)}{N \sin(\pi\tau_o f)}\right]^2 df \qquad (4\text{-}15)$$

It can be shown [10] that the value of the integral in equation (4-15) is given by

$$B_{NP} = \frac{1}{2N\tau_o} \qquad (4\text{-}16)$$

If a flat input noise power spectrum η is assumed, the input variance is given by

$$\sigma_{in}^2 = \eta B_{IN}$$

$$= \frac{\eta}{2\tau_o} \qquad (4\text{-}17)$$

Substituting equation (4-16) into equation (4-17) a result equivalent to the result of equation (3-10) is obtained.

$$\sigma_N^2 = \eta B_{NP} = \frac{\eta}{2N\tau_o}$$

$$\sigma_N^2 = \frac{\sigma_{in}^2}{N} \qquad (4\text{-}18)$$

Clearly, the assumption of a flat input power spectrum at this point in the frequency domain approach is equivalent to the assumption of statistical independence of samples in equation (3-10).

The input post-loop samples are not statistically independent, or from the frequency domain point of view, the input power spectrum is not flat. The input noise spectrum is shaped before reaching the post-loop processor by the power transfer function of the loop. The loop relative amplitude-squared frequency response function $A_L^2(f)$ has been determined to be

$$A_L^2(f) = \frac{|H_{CL}(f)|^2}{H_{CL\ max}^2}$$

$$= \frac{1}{1 + \left(\frac{2\pi f}{50}\right)^2}$$

$$= \frac{1}{1 + \left(\frac{f}{7.96}\right)^2} \qquad (4\text{-}19)$$

In order to determine the effect of the post-loop processor on statistically dependent samples, the effect of the loop process $A_L^2(f)$ on the power spectrum of the post-loop processor input must be examined. The noise bandwidth of the combination of the loop response and the post-loop processor is found to be

$$B_{NO} = \int_0^{1/2\tau_o} \left[\frac{\sin\ (N\pi f\tau_o)}{N\ \sin\ (\pi f\tau_o)}\right]^2 \frac{1}{1 + \left(\frac{f}{7.96}\right)^2}\, df \qquad (4\text{-}20)$$

Letting $x = \tau_o f$ equation (4-20) becomes

$$B_{NO} = \frac{1}{N\tau_o} \int_0^{1/2} \left[\frac{\sin(N\pi x)}{\sin(\pi x)}\right]^2 \frac{dx}{1 + \left(\frac{x}{0.214}\right)^2} \qquad (4\text{-}21)$$

Equation (4-21) was evaluated numerically, and the results are shown in table 4-1 for selected values of N.

TABLE 4-1

EFFECTIVE NOISE BANDWIDTHS OF POST-LOOP PROCESSOR OUTPUTS

N		1	2	4	8	16	32	64
$B_{NO}N\tau_o$		0.3326	0.3459	0.4177	0.4586	0.4793	0.4896	0.4948
B_{NO}		12.5 Hz	6.49 Hz	3.92 Hz	2.15 Hz	1.12 Hz	0.574 Hz	0.290 Hz

The sensitivity of the proposed digital signal processing radiometer can be determined using the expression for the sensitivity given in equation (2-16), and the output equivalent noise bandwidths for the control-loop and post-loop processor are listed in table 4-1. From equation (2-16), the sensitivity ΔT of the closed-loop noise injection radiometer is given as

$$\Delta T = 1870\sqrt{\frac{2B_{NO}}{B_{SI}}} \qquad (4\text{-}22)$$

where B_{NO} is the output equivalent noise bandwidth and B_{SI} is the input statistical bandwidth. The sensitivity of the proposed design can now be found by substituting the output noise bandwidths for the various

post-loop outputs, listed in table 4-1, into equation (4-22). These sensitivities are listed in table 4-2.

TABLE 4-2

SENSITIVITY AND REQUIRED MEASUREMENT TIME FOR

DIGITAL PROCESSING RADIOMETER

B_{SI}	N	1	2	4	8	16	32	64
20 MHz	ΔT (IN K)	2.09	1.51	1.17	0.867	0.626	0.448	0.318
	τ_s (IN s)	0.160	0.187	0.240	0.320	0.533	0.960	1.79
100 MHz	ΔT (IN K)	0.935	0.674	0.524	0.388	0.280	0.200	0.142
	τ_s (IN s)	0.187	0.187	0.240	0.347	0.560	0.960	0.813
500 MHz	ΔT (IN K)	0.418	0.301	0.234	0.173	0.125	0.0896	0.0637
	τ_s (IN s)	0.187	0.213	0.267	0.347	0.560	0.987	1.82
2 GHz	ΔT (IN K)	0.209	0.151	0.117	0.0867	0.0626	0.0448	0.0318
	τ_s (IN s)	0.313	0.240	0.267	0.373	0.587	0.986	1.80

In order to compare the sensitivities listed in table 4-2 to the corresponding values for the analog system, the measurement time of the digital process must be defined. The step response of the control loop is determined from equation (4-7) to be

$$y(n\tau_s) = C(T_B - T_A)(1 - e^{-50n\tau_s}) \qquad (4\text{-}23)$$

where τ_s is the loop sample rate $\left(\tau_s = \frac{1}{16}\tau_o\right)$. The average based on N samples in the post-loop processor is

$$y_N(k\tau_o) = \frac{1}{N}\sum_{n=k}^{k-N+1} y(n\tau_o)$$

$$= C(T_B - T_A)\left[1 - \frac{1}{N}\sum_{n=0}^{N-1} e^{-50(k-n)\tau_o}\right] \qquad (4\text{-}24)$$

where $y_N(k\tau_o)$ is the output of the post-loop processor at $k\tau_o$ (τ_o is the sample time based on the post-loop sample rate). The error Δy_N of the step response is determined from equation (4-24) to be

$$\Delta y_N(k\tau_o) = C\,\frac{(T_B - T_A)}{N}\sum_{n=0}^{N-1} e^{-50(k-n)\tau_o} \qquad (4\text{-}25)$$

If the settling time is again defined as the time when the error due to the finite settling time is less than 10 percent of the fluctuation error, then

$$\Delta y_N(k_s\tau_o) = \frac{\Delta T}{10} = (T_B - T_A)\,\frac{1}{N}\sum_{n=0}^{N-1} e^{-50(k_s-n)\tau_o} \qquad (4\text{-}26)$$

where $k_s\tau_o$ equals the settling or measurement time for the y_N post-loop output. The worst conditions for the settling time occur when $T_A = 0.0$ K and when the first sample is taken just as the input step goes high. Under these conditions, the settling time is

$$\tau_s(N) = k_s\tau_o = \frac{-1}{50}\,\ell n\left[\frac{N\Delta T(N)}{3080}\left(\frac{1 - e^{50\tau_o}}{1 - e^{50\tau_o N}}\right)\right] \qquad (4\text{-}27)$$

where $\Delta T(N)$ is the sensitivity of the y_N post-loop output and $\tau_s(N)$ is the settling time of the y_N output. The settling times for each of

the post-loop processor outputs have been calculated using equation (4-27) and are listed with the appropriate sensitivities in table 4-2. A graph of required settling time versus sensitivity for the digital processing radiometer is presented in figure 4-2.

Of interest also is the level of the Dicke ripple. While the odd harmonics of the Dicke switch frequency are eliminated by the accumulator as described in Chapter III, even harmonics will be generated due to the noise injection pulses. Consider the block diagram of the radiometer in figure 2-5, and the corresponding error voltage waveform at the output of the **correlator illustrated in figure 4-3.** Due to the linearity of the Fourier operator, the even harmonics of this asymmetric waveform can be considered to originate from a pulse train at the Dicke frequency, with duty cycle $\frac{d}{2}$, where $d = \frac{t_1}{\tau}$ is defined as the ratio of the time of the injected noise to one-half the Dicke period (see figure 4-3). The magnitudes V_N of the sine-cosine Fourier expansion of this pulse train can be expressed as

$$V_N = 2\left(\frac{d}{2}\right) T_I K_1 |G(j\omega_N)| \frac{\sin\left(\frac{N\pi d}{2}\right)}{\frac{N\pi d}{2}} \qquad (4\text{-}28)$$

The accumulator algorithm eliminates the odd harmonics, the notch filter eliminates the 600 Hz component, and the loop response attenuates the higher order even harmonics. Thus, the most significant component of the Dicke ripple is the fourth harmonic

$$V_4 = \frac{T_I}{2\pi}\left[K_1 |G(j\omega_4)|\right]\left[\sin\ (2\pi d)\right] \qquad (4\text{-}29)$$

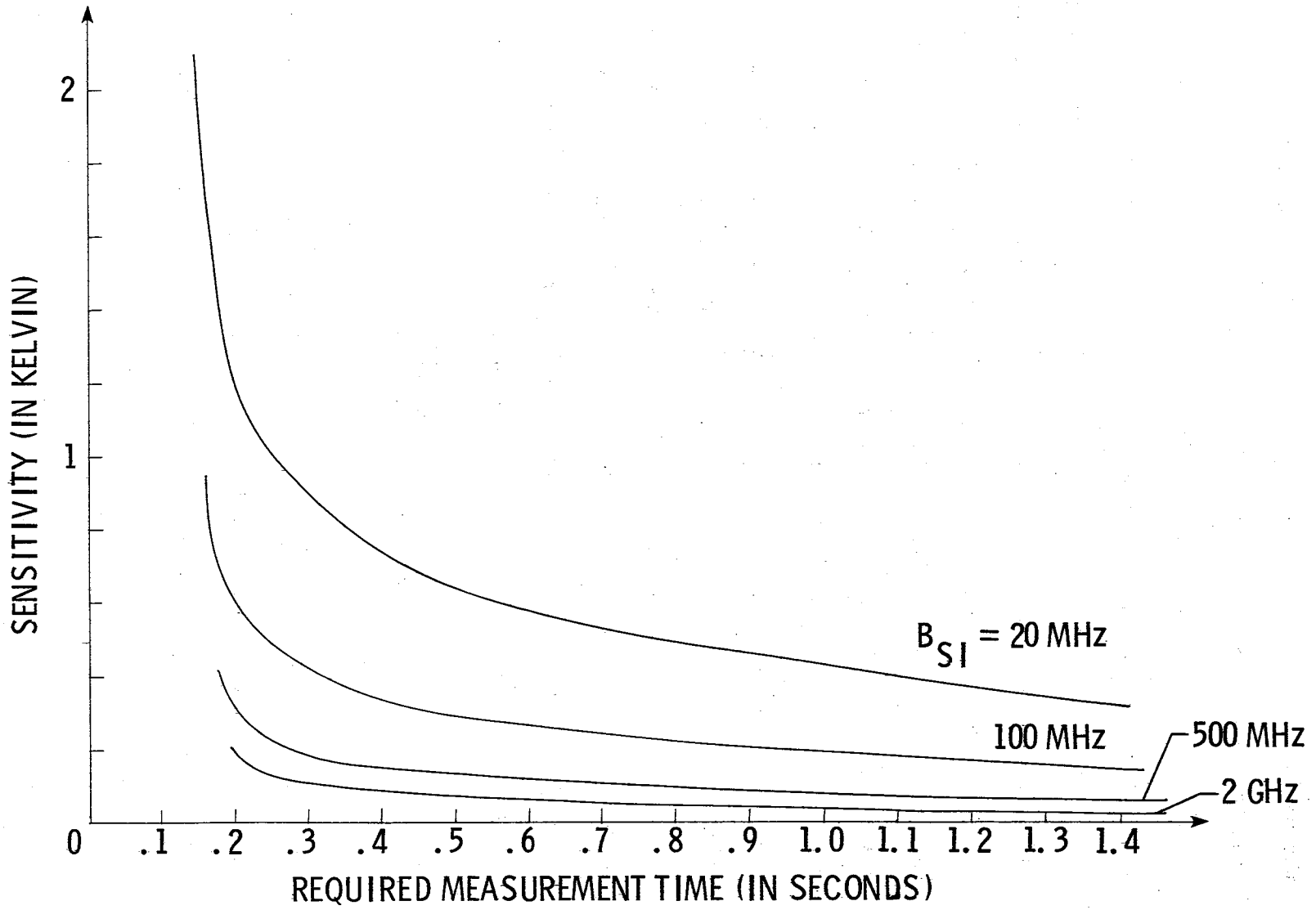

Figure 4-2. Measurement time versus sensitivity for proposed design.

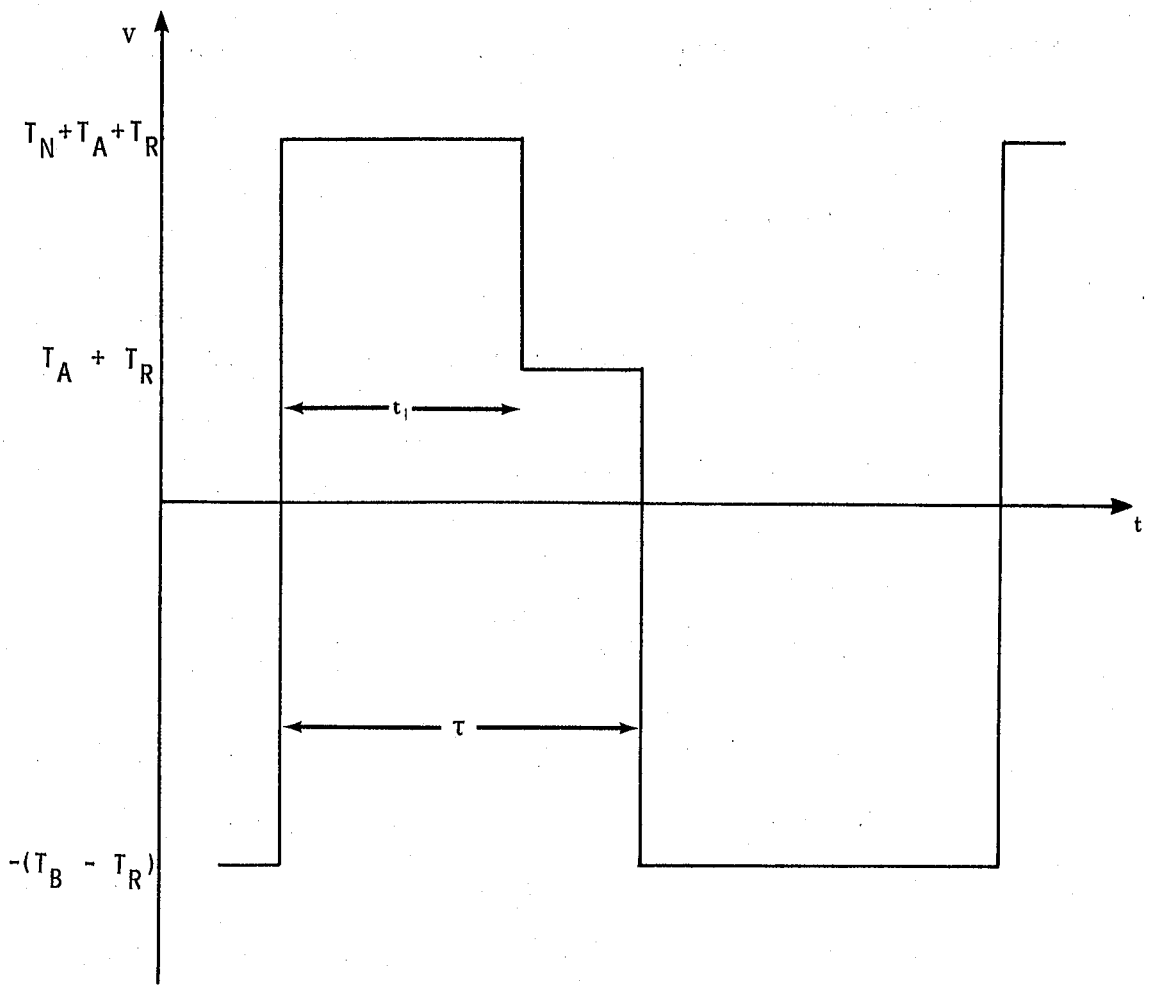

Figure 4-3. Error voltage waveform for digital processing radiometer.

The desired signal, i.e., the dc output level of the accumulator, is given by

$$V_o = \frac{T_B - T_A}{K_2} \tag{4-30}$$

The ripple factor ρ expresses the output peak ripple as a percentage of the dc output.

$$\rho = \frac{V_4}{V_o} \times 100\%$$

$$\rho = \frac{T_I}{2\pi(T_B - T_A)} K_1 K_2 |G(j\omega_4)| \sin(2\pi d) \times 100\% \tag{4-31}$$

Substituting the appropriate value for the loop gain equation (4-31) becomes

$$\rho = \frac{9.78 \times 10^{-4}}{2\pi(308 - T_A)} \sin\left[2\pi\left(\frac{308 - T_A}{368.08}\right)\right] \times 100\% \tag{4-32}$$

This ripple factor versus input temperature is plotted in figure 4-4. The Dicke ripple level within the digital radiometer is far below the ripple in the analog radiometer. In addition to the reduction in the level of the Dicke ripple, the digital signal processor is also more efficient than the analog unit in that it can form a measurement of the same sensitivity as the analog radiometer in less time. In the following chapter a more detailed comparison between the analog and digital signal processors will be made.

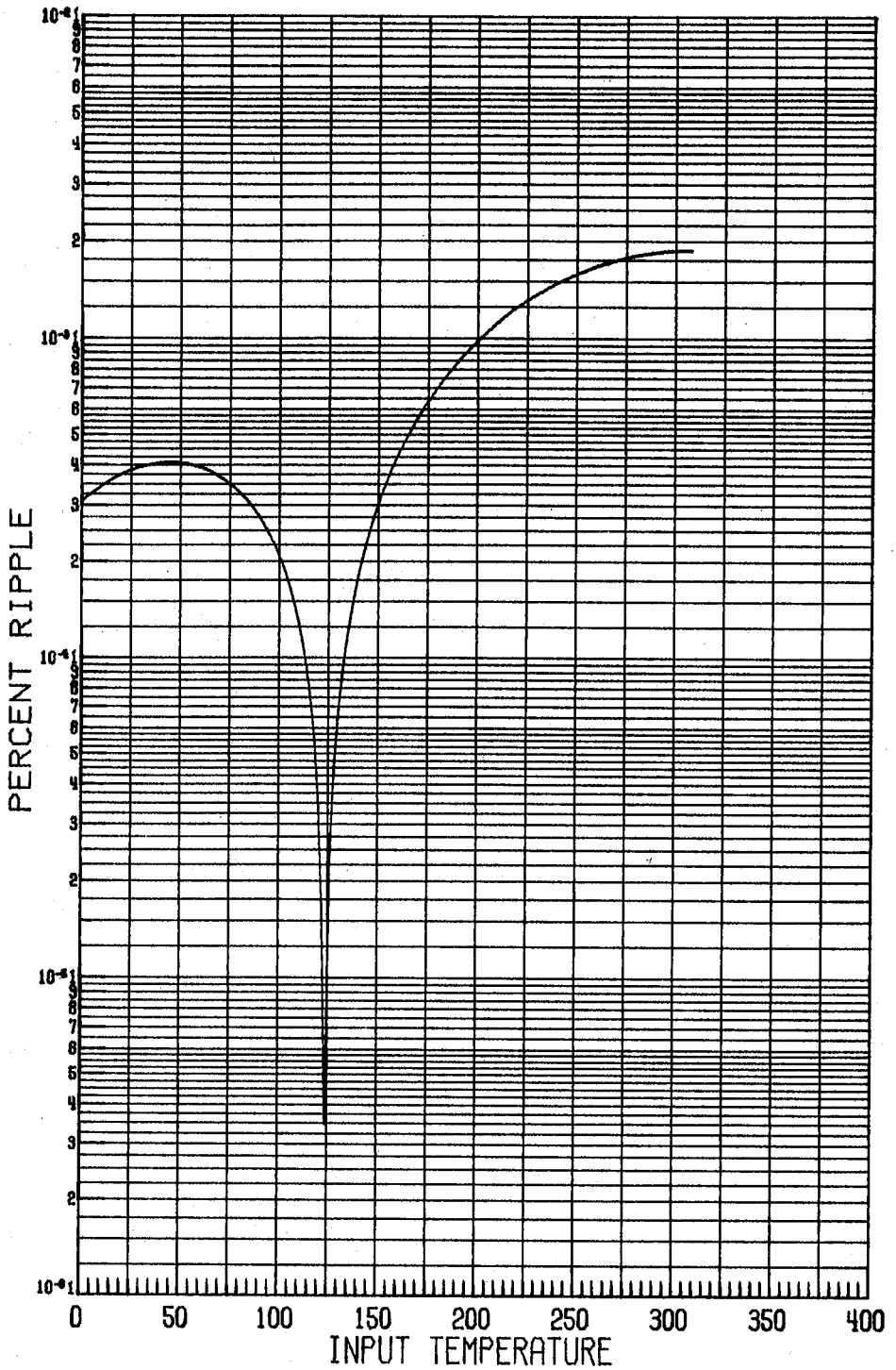

Figure 4-4. Ripple factor versus antenna temperature for proposed radiometer.

B. Experimental

A prototype version of the digital signal processor has been implemented on an Intel 8086 microprocessor evaluation system. The digital processor is shown in the user breadboard area of the evaluation system illustrated in figure 4-5. Only a small fraction of the support chips and memory available in the evaluation system were actually used by the digital processor. However, the monitor program and thorough documentation available for the evaluation system made it ideal for the first realization attempt. The prototype digital processor was then interconnected with the existing radiometer so that it replaced the existing analog estimation and averaging sections (see figure 4-6). The digital processor was tested for proper operation as a part of the radiometer. The output of the video amplifier for the radiometer with the analog processor is shown in figure 4-7(a). The Dicke switching process can easily be seen. The noise injection pulses can also be seen during the antenna portion of the Dicke switch cycle. The output of the video amplifier with the digital processor inserted is shown in figure 4-7(b). The noise injection pulse can clearly be seen in the first part of the antenna portion of the Dicke switch cycle. The step response of the analog radiometer [10] is shown in figure 4-8(a). Note the Dicke ripple seen in the response. The step response of the digital processing radiometer is shown in figure 4-8(b). From figure 4-8 it can be seen that the Dicke ripple has been reduced significantly.

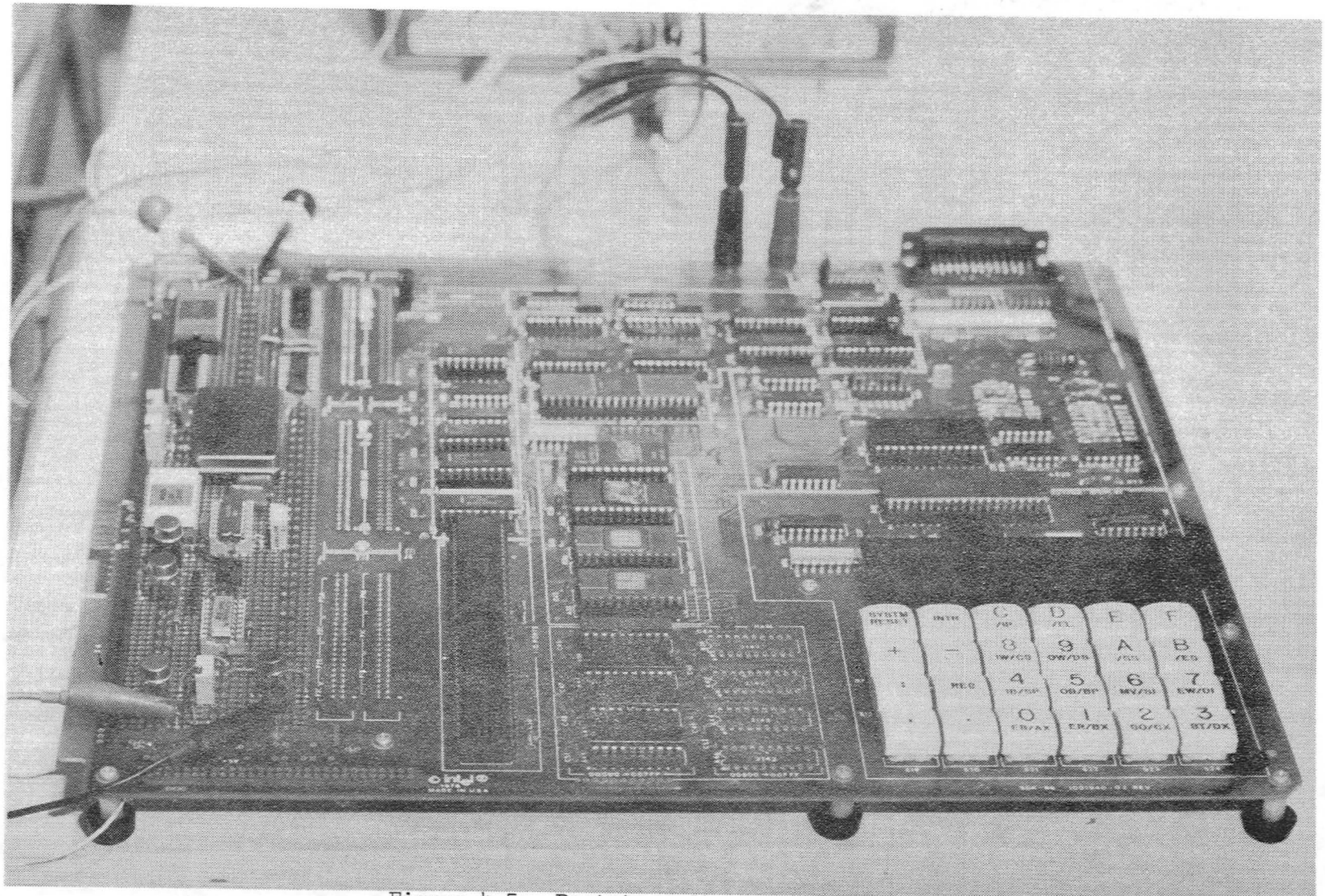

Figure 4-5. Prototype digital processor.

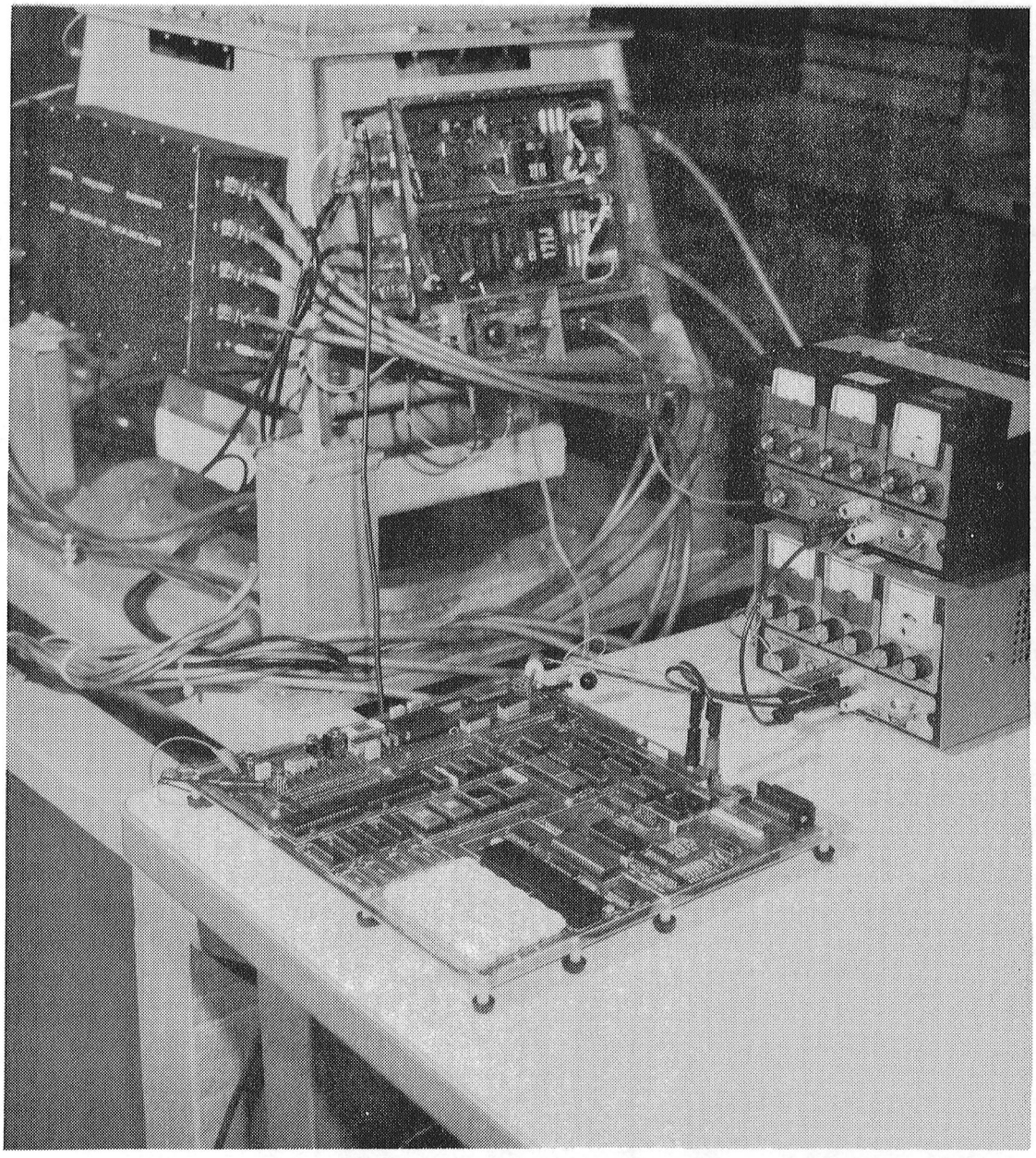

Figure 4-6. Digital processor and existing radiometer in test configuration.

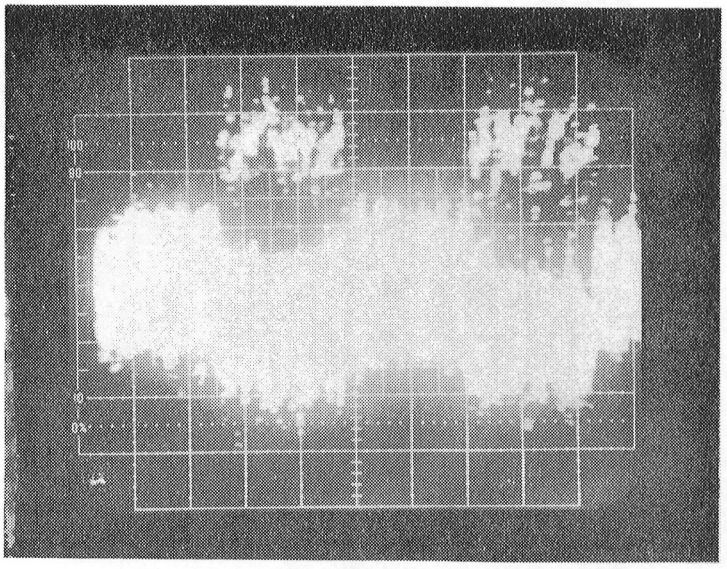

(a)

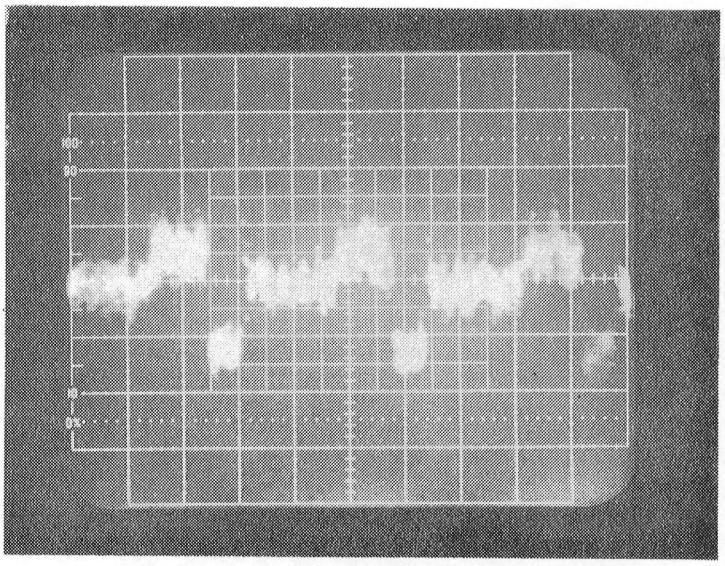

(b)

Figure 4-7. Video amplifier output of analog and digital processing radiometers.

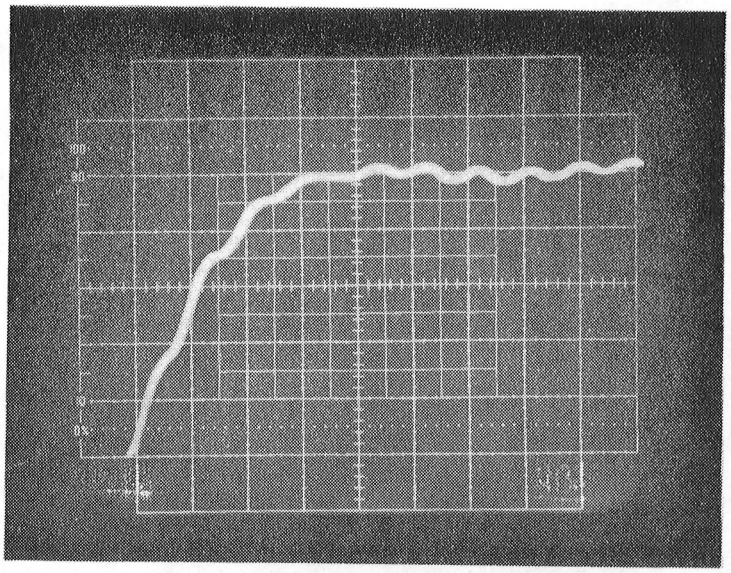

(a)

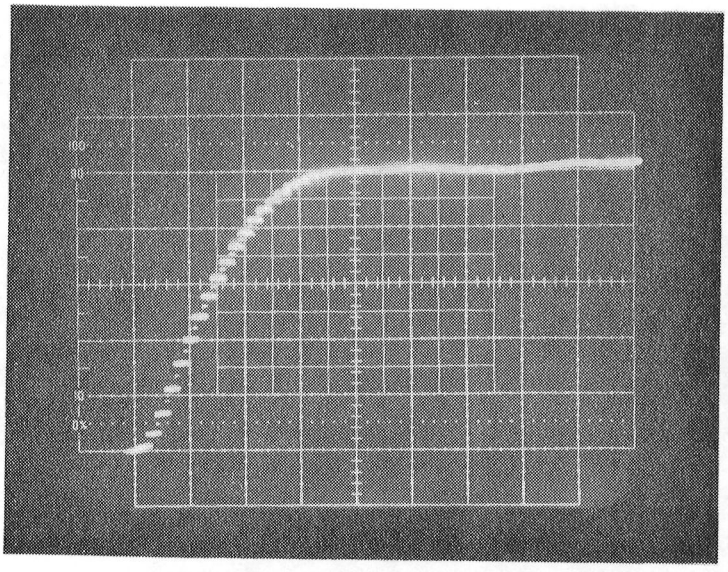

(b)

Figure 4-8. Step response of analog and digital processing radiometers.

The radiometer has been installed on an aircraft, and data were recorded in flight with both analog and digital signal processors. Results of this test flight are very encouraging. Analyses performed on these test data thus far indicate that the digital processing radiometer is operating as predicted.

CHAPTER V

CONCLUSIONS

The purpose of this research was to develop an improved power estimation strategy for a Dicke switching noise injection radiometer. It was shown that the Dicke ripple inherent in the Dicke switching process within the analog radiometer could be eliminated using sample data techniques. Elimination of the ripple allowed the use of a faster responding control loop. The resulting decreased settling time leads to an increased number of uncorrelated samples at the loop output, thus allowing most of the averaging to be performed in a post-loop processor. The flexibility and efficiency of this post-loop averaging result in an improved estimation strategy. A comparison of the radiometer using the proposed processing technique and the original analog radiometer is presented below in support of the improved performance.

A. Dicke Ripple

An expression for the Dicke ripple level as a percentage of the desired dc signal was determined for both the digital and analog processors in previous chapters. It was determined that this ratio was a function of antenna temperature. A graph of the ratio of the ripple level to dc level (or ripple factor) versus antenna temperature is shown in figure 5-1. In this graph, the ripple factors for the digital and analog processes are shown on the same scale. The reduction in the ripple level due to the elimination of the odd harmonics of the Dicke frequency by the accumulator can clearly be seen.

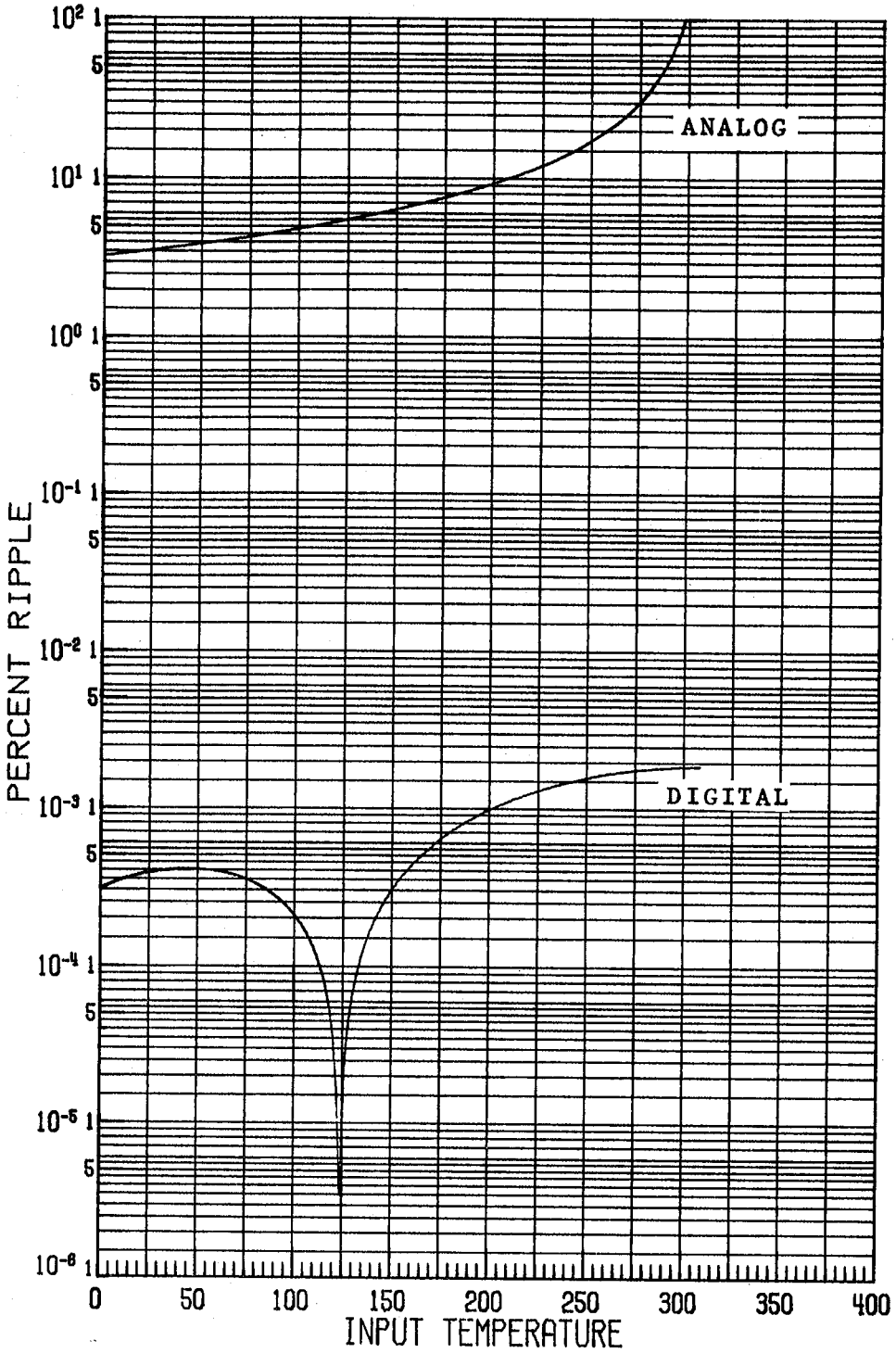

Figure 5-1. Comparison of ripple factor.

This reduction in Dicke ripple is significant since it permits the control loop to have reduced settling time. This fast settling time is available since the loop is no longer required to attenuate the Dicke ripple.

B. Sensitivity

As explained in Chapter II longer integration times produce a more sensitive measurement of a larger area (less spatial resolution). It is then desired to perform the measurement to the required sensitivity in the shortest possible time. Thus, in order to compare the sensitivity of the analog and digital radiometers, the time required to form the measurement must be considered. The y_2 post-loop output, or the average of two loop output samples, has approximately the same theoretical sensitivity as the original analog radiometer. The times required to form the measurement of these sensitivities for the available input bandwidths are shown for the analog and the y_2 post-loop output of the digital processing radiometer in figure 5-2. From figure 5-2, it can be clearly seen that the digital processing radiometer is superior to the analog unit in that it can provide a measurement with the same sensitivity as the analog processor in less time. This results in better spatial resolution.

C. Spatial Resolution

For a specified spatial resolution the total error in the estimate of the brightness temperature is made up of fluctuation error and "antenna smear" error. Longer integration times will reduce the

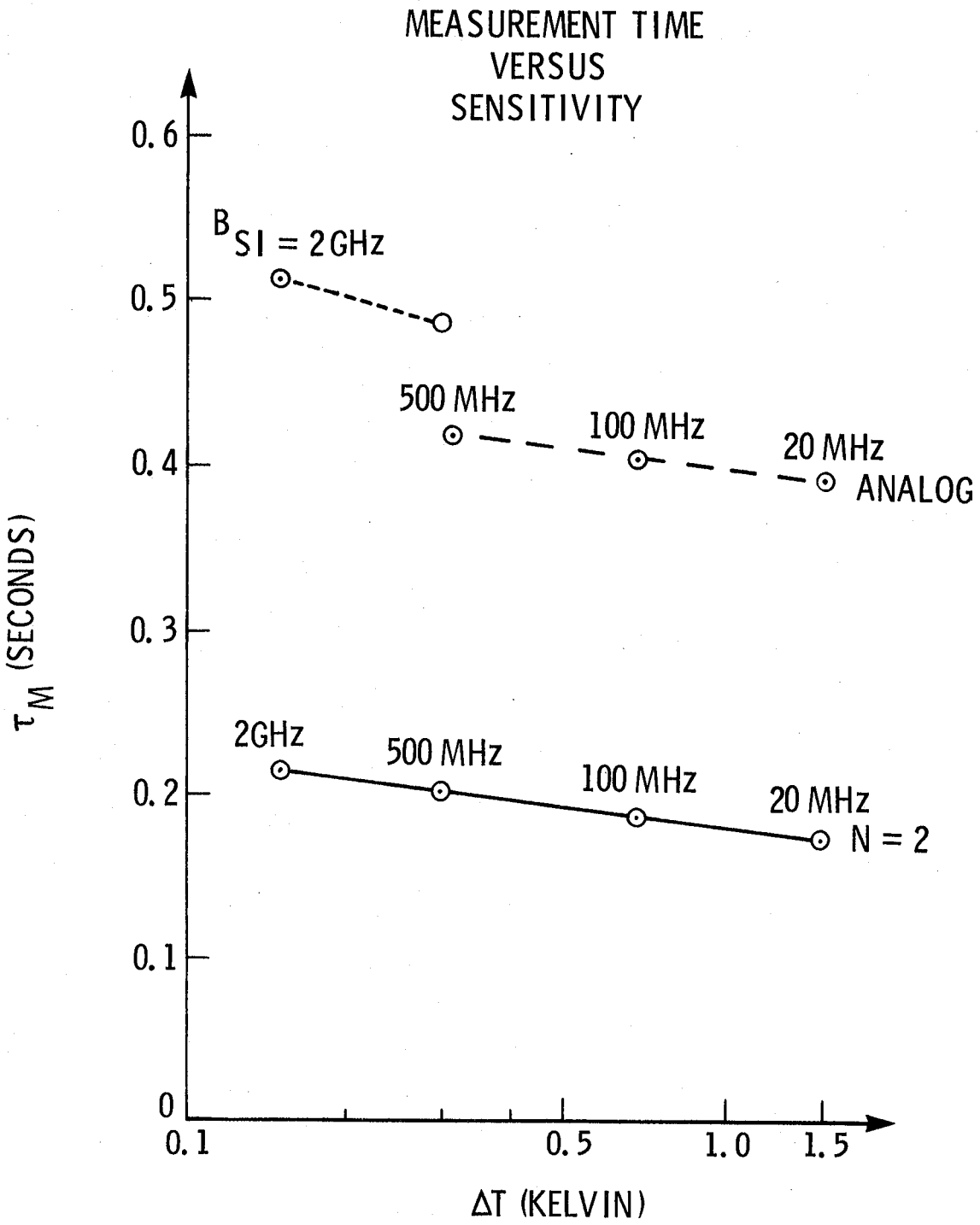

Figure 5-2. Comparison of required measurement time.

fluctuation error ΔT. However, longer integration times will degrade the spatial resolution, due to the measurement platform movement, thus increasing the "antenna smear" error given in equation (2-15). Examination of equation (2-15) reveals that the "antenna smear" error is a function of the brightness temperature. Referring to equation (2-15) it can be seen that if the radiometer is moving over a scene in which the brightness temperature changes slowly, it is possible to increase the integration time with little increase in the "antenna smear" error. However, as the radiometer approaches a point where the brightness temperature changes rapidly (such as an ice/water boundary), the integration time must be reduced to limit the "antenna smear" error.

An advantage of the digital processing radiometer is that the measurement is made to several sensitivities simultaneously, and these estimates are available simultaneously at the various post-loop outputs. Thus, an operator can determine which post-loop output will provide the best estimate of the brightness temperature for a particular type of scene and specified spatial resolution. More specifically, for a desired spatial resolution, there is an optimum integration time which will minimize the total adverse effects due to fluctuation errors and the "antenna smear" error. This decision must be made by the operator with the present system. However, the antenna footprint size and aircraft speed may be such that it could be possible to approximate the infinite sum of equation (2-15) by the first few terms of the series. This would result in an approximation of the "antenna smear" error for a particular footprint size, aircraft speed, and scene. Then, using the

radiometer's estimate of the scene, a continual approximation of the "antenna smear" error could be formed. If this is possible, the microprocessor program could determine the optimum integration time for a particular required spatial resolution. Thus, the radiometer could continually adjust the integration time as the scene varies by selecting the appropriate post-loop output such that the output is the best estimate of the scene for the required spatial resolution. This varying integration time scheme is presented here to demonstrate the desirability of the added flexibility obtained using the digital processor. Although no further investigation was attempted at this time, it is suggested as a topic for future research.

D. Summary

The digital signal processing radiometer presented here is superior to the original analog system in several respects. The Dicke ripple due to the modulation and demodulation processes within the radiometer is substantially reduced by the digital signal processor, thus enabling the use of the post-loop processing technique. The time required to form a measurement to a specified sensitivity is shorter for the digital processing radiometer. This reduction in required measurement time is actually due to the more optimum loop design and post-loop averaging, and is not specifically a result of the digital techniques used. However, the subsequent reduction in measurement time is significant since it results in a more sensitive radiometer. The added flexibility obtained by use of the digital techniques may also lead to improved

radiometer performance. Thus, the objective of this investigation, i.e., the development of a power estimation strategy demonstrating performance superior to the original design has been accomplished.

LIST OF REFERENCES

1. Bendat, J. S.; and Piersol, A. G.: Random Data: Analysis and Measurement Procedures. John Wiley & Sons, Inc., 1971.

2. Collin, R. E.: Antenna Theory. McGraw-Hill, Inc., 1969.

3. Collin, R. E.: Foundation for Microwave Engineering. McGraw-Hill, Inc., 1966.

4. Dicke, R. H.: The Measurement of Thermal Radiation at Microwave Frequencies. The Review of Scientific Instruments, Vol. 17, No. 7, July 1946, pp. 268-275.

5. Kraus, J. D.: Radio Astronomy. McGraw-Hill, Inc., 1966.

6. Lawrence, R. W.; Stanley, W. D.; and Harrington, R. F.: Digital Signal Processing in Microwave Radiometers. Paper presented at the 1980 IEEE Southeastcon, Nashville, Tennessee, April 1980.

7. Rainwater, J. H.: Radiometers: Electronic Eyes That "See" Noise. Microwaves, September 1978, pp. 58-62.

8. Stanley, W. D.: Digital Simulation of Dynamic Processes in Radiometer Systems. Old Dominion University Research Foundation Report, NAS1-14193 Task 46, May 1979.

9. Stanley, W. D.; Harrington, R. F.; and Lawrence, R. W.: Dynamic Simulation of Random Processes in Radiometers Using CSMP and ASCL. Paper presented at the 1979 IEEE Southeastcon, Roanoke, Virginia, April 1979.

10. Stanley, W. D.: Preliminary Development of Digital Signal Processing in Microwave Radiometers. Old Dominion University Research Foundation Report NAS1-15676, 1979.

11. Tiuri, M. E.: Radio Astronomy Receivers. IEEE Transactions on Antennas and Propagation, Vol. AP-12, No. 4, December 1964, pp. 930-938.

12. Wait, D. F.: The Sensitivity of the Dicke Radiometer. Journal of Research of the National Bureau of Standards, Vol. 71C, No. 2, April-June 1967, pp. 127-152.

13. Watson, H. A.: Microwave Semiconductor Devices and Their Circuit Application. McGraw-Hill, Inc., 1969.

APPENDIX A

OVERVIEW OF THE DICKE RADIOMETER

A radiometer is a precise instrument which measures electromagnetic energy radiated from a surface. Any object will emit a particular broadband spectrum of electromagnetic energy depending on its temperature and physical characteristics such as emissivity. Max Planck established that the emission spectrum of a hypothetical blackbody is completely governed by its absolute physical temperature [7]. The power spectrum of a blackbody with an absolute temperature T can be expressed by

$$P = \frac{2hf^3}{c^2}\left[\exp(hf/kT) - 1\right]^{-1} \Delta f \, d\Omega \qquad \text{(A-1)}$$

where

P = power radiated into solid angle $d\Omega$ in bandwidth Δf, W

h = Planck's constant = 6.63×10^{-34} J·s

f = frequency, Hz

c = velocity of light, m/s

k = Boltzmann's constant = 1.38×10^{-23} J/K

T = absolute physical temperature, K

In the microwave frequency region, for most practical situations, the term hf/kT is sufficiently small that the exponential function can be approximated by the first term of its Taylor expansion; i.e., $\exp(hf/kT) \approx 1 + (hf/kT)$. The power radiated by the blackbody can then be expressed as

$$P = \frac{2kT}{\lambda^2} \Delta f \, d\Omega \tag{A-2}$$

where $\lambda = c/f$.

An ideal "lossless" linearly polarized antenna with receiving cross section $A(\Omega)$ viewing a blackbody receives a power P_R given by

$$P_R = \frac{1}{2} \int_{\Omega} \frac{2kT \, \Delta f}{\lambda^2} A(\Omega) \, d\Omega \tag{A-3}$$

where the factor of one-half is due to the fact that the antenna receives energy in only one plane of polarization [7].

It can be shown [2] that

$$\begin{aligned} \int_{\Omega} A(\Omega) \, d\Omega &= \frac{\lambda^2}{4\pi} \int_{\Omega} G(\Omega) \, d\Omega \\ &= \frac{\lambda^2}{4\pi} (4\Pi) \\ &= \lambda^2 \end{aligned} \tag{A-4}$$

where $G(\Omega)$ is the absolute antenna gain function. Combining equations (A-3) and (A-4) results in

$$P_R = kT \, \Delta f \tag{A-5}$$

Rearranging equation (A-5),

$$T = \frac{P_R}{k \, \Delta f} \tag{A-6}$$

The quantity T is called the antenna temperature, which will subsequently be denoted as T_A. The value T_A corresponds to the temperature

that a blackbody must have at the antenna terminals to produce the received power P_R. The rationale for the common practice of referring to a noise power distribution as an equivalent noise temperature is illustrated by equation (A-6).

In practice, the object of interest is not a blackbody. Thus, the received power is not solely a function of the physical temperature, but is also a function of the emissivity, reflected radiation, and atmospheric path. This investigation only considered the problem of accurately measuring the antenna output power or antenna temperature T_A. The problem of determining properties of the object from the measurement of T_A was not considered.

The output signal from the antenna is actually low level gaussian noise with zero mean. The radiometer must estimate the variance or noise power of this signal. Measuring the variance of this signal presents several interesting problems. One problem is that the actual level of the received signal is extremely low and is often smaller than the receiver noise. The antenna temperatures of interest range from 100 to 270 K, corresponding to a received power density of 1.38×10^{-21} to 3.73×10^{-21} W/Hz. In comparison, the noise generated within the radiometer referred to the input is approximately 627 K, corresponding to a receiver noise power density of 8.65×10^{-21} W/Hz. Thus, the desired signal appears to be obscured by the higher level receiver noise. Also, due to the extremely low level of these signals, substantial amplification will be required before any attempt can be made to measure the level of the received power. The amplifiers used to

provide this gain must be very stable since changes in the gain will cause changes in the measured signal power. Thus, in order to measure the power of the received signal, the receiver noise and the gain of the radiometer must be precisely known and extremely stable. Any uncertainty in the receiver noise power or the gain will result in an erroneous measurement of the received signal power.

The Dicke switching noise injection radiometer shown in figure A-1 is one system used to measure the power of the received signal while reducing errors due to the previously mentioned problems. A brief introduction to the basic operation of this radiometer will now be presented. Referring to figure A-1, the input to the radio frequency (RF) amplifier is switched between a known noise temperature T_B and the antenna output plus feedback injected noise $T_A + T_F$. This switched signal passes through the RF amplifier and input filter where it is corrupted by the receiver noise T_R. Thus, the output of the filter switches between two zero mean gaussian distributed noise signals, one with variance proportional to $T_B + T_R$, and the other with variance proportional to $T_A + T_F + T_R$.

The output of the filter is applied to the square-law detector. If the input to the square-law detector is a random process $x(t)$, then the output is given by

$$y(t) = x^2(t) \tag{A-7}$$

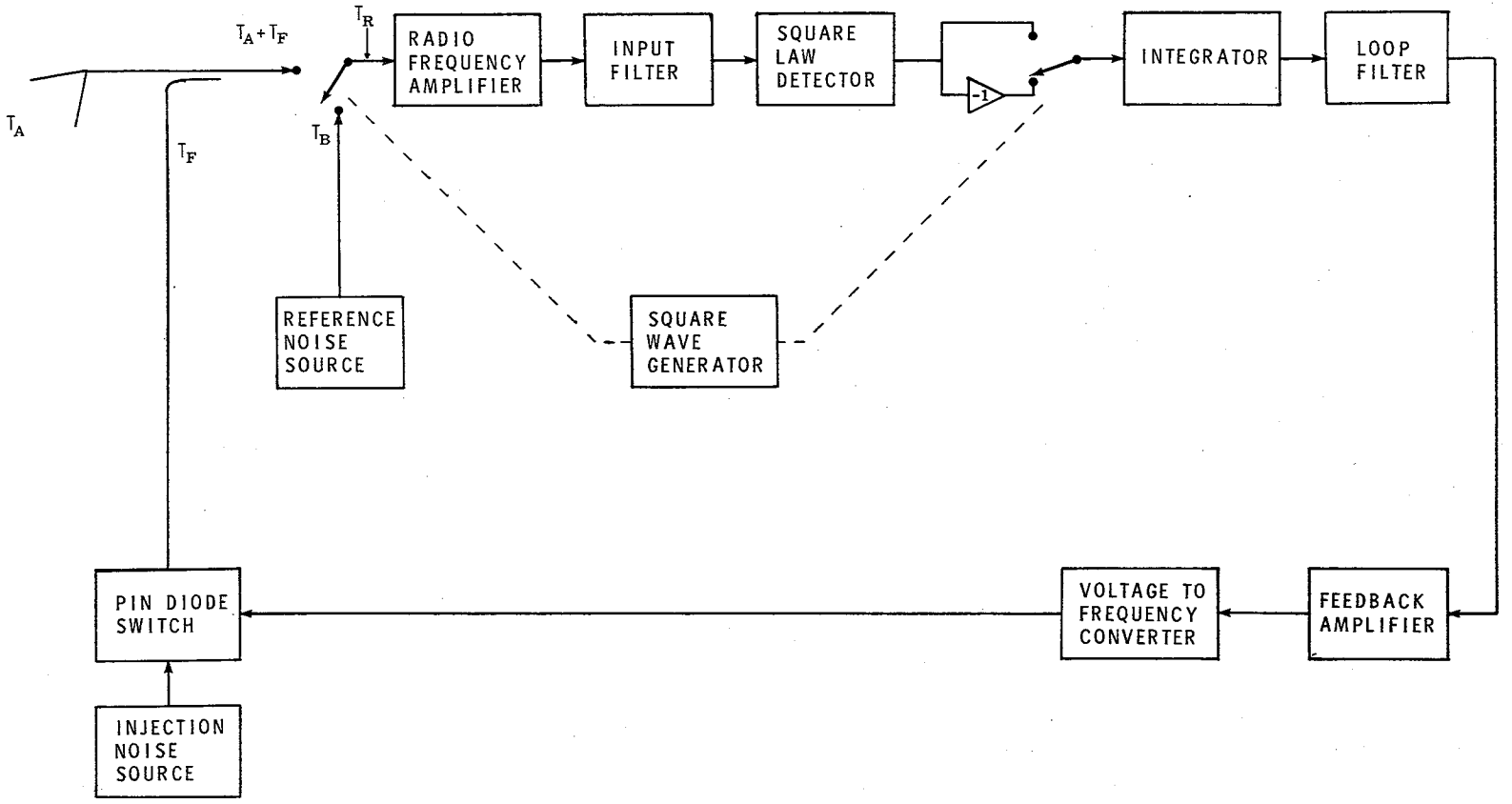

Figure A-1. Dicke switching noise injection radiometer.

The mean of $y(t)$ is given by

$$\mu_y(t) = E\{x^2(t)\}$$

$$\mu_y(t) = \left[E\{x(t)\}\right]^2 + \sigma_x^2(t) \qquad \text{(A-8)}$$

$$\mu_y(t) = \mu_x^2(t) + \sigma_x^2(t)$$

Since $\mu_x(t) = 0$, equation (A-8) can be reduced to

$$\mu_y(t) = \sigma_x^2(t) \qquad \text{(A-9)}$$

Thus, if the input to the square-law detector has zero mean, the mean value of the output of the square-law detector equals the variance or power of the input. The input to the square-law detector is switched between two zero mean random variables, one with variance proportional to $T_B + T_R$ and the other with variance proportional to $T_A + T_F + T_R$. Thus, from equation (A-9), the output of the square-law detector switches between two random variables, one with mean proportional to $T_B + T_R$, and the other with mean proportional to $T_A + T_F + T_R$. The output of the square-law detector is switched in synchronization with the input switch such that the signal is alternately connected directly to the integrator and then inverted before being connected to the integrator. When both switches are up, the integrator "sees" a random variable with mean proportional to $T_A + T_F + T_R$. When both switches are down, the integrator "sees" a random variable with mean proportional to $-(T_B + T_R)$. The estimation and averaging section then estimates the

mean (i.e., dc value) of this random variable. The mean of the signal over a full switching cycle is given by

$$\mu_e = C\left[(T_A + T_F + T_R) - (T_B + T_R)\right]$$
$$\mu_e = C(T_A + T_F - T_B) \tag{A-10}$$

where C is a system constant. It can be seen from equation (A-10) that the receiver noise does not contribute to the net mean value of the input to the estimation and averaging section. Thus, the Dicke switching process effectively eliminates the need to know the value of T_R, as well as the uncertainty in the measurement due to fluctuations of T_R.

The output of the estimation and averaging section is then used to control the injected noise. Since the noise temperatures of the reference source T_B and injected noise T_F are known, an estimate of T_A can be made from the result of equation (A-10). This estimate is used to adjust the injected noise power such that $T_F = T_B - T_A$. The mean value of the input to the estimation and averaging section (or loop error signal) as determined from equation (A-10) then becomes

$$\mu_e = C\left[(T_A + T_F + T_R) - (T_B + T_R)\right]$$
$$\mu_e = C\left[(T_A + (T_B - T_A) + T_R) - (T_B + T_R)\right]$$
$$\mu_e = C\left[(T_B + T_R) - (T_B + T_R)\right] \tag{A-11}$$
$$\mu_e = 0.$$

Thus, the mean value of the random variable input to the estimation and averaging section is zero, and the control loop is locked. This feedback concept will automatically compensate for fluctuations in the forward loop gain since such changes will not affect the final value of the loop. Thus, the Dicke noise injection radiometer has eliminated the effect of the receiver noise power and has reduced errors caused by fluctuations in the forward loop receiver gain.

APPENDIX B

IMPLICATIONS OF TIME AVERAGING A NONERGODIC PROCESS

In order to determine what the time average of the output of the square-law detector implies about the ensemble average, consider the random process $y(t)$ at the output of the square-law detector. Let $\hat{\mu}_y(t)$ represent the time average of $y(t)$, and let

$$y(t) = \mu_y(t) + z(t) \tag{B-1}$$

where $z(t)$ is a random process with zero mean, and $\mu_y(t)$ is the mean value of $y(t)$ corresponding to the brightness temperature. The time average of the output of the square-law detector is then determined to be

$$\hat{\mu}_y(t) = \frac{1}{\tau}\int_{t-\tau/2}^{t+\tau/2} y(\zeta)\, d\zeta$$

$$\hat{\mu}_y(t) = \frac{1}{\tau}\int_{t-\tau/2}^{t+\tau/2} \left[\mu_y(\zeta) + z(\zeta)\right] d\zeta \tag{B-2}$$

If this time average is an unbiased estimate of $\mu_y(t)$, i.e., the scene brightness temperature, then $E\{\hat{\mu}_y(t)\}$ should equal the brightness temperature $B(t)$. Taking the ensemble average of both sides of equation (B-2) results in

$$
\begin{aligned}
E\{\hat{\mu}_y(t)\} &= E\left\{\frac{1}{\tau}\int_{t-\tau/2}^{t+\tau/2}\left[\mu_y(\zeta) + z(\zeta)\right]\, d\zeta\right\} \\
E\{\hat{\mu}_y(t)\} &= \frac{1}{\tau}\int_{t-\tau/2}^{t+\tau/2} E\{\mu_y(\zeta)\} + E\{z(\zeta)\}\, d\zeta \\
E\{\hat{\mu}_y(t)\} &= \frac{1}{\tau}\int_{t-\tau/2}^{t+\tau/2} E\{\mu_y(\zeta)\}\, d\zeta \\
E\{\hat{\mu}_y(t)\} &= \frac{1}{\tau}\int_{t-\tau/2}^{t+\tau/2} B(\zeta)\, d\zeta \neq B(t)
\end{aligned}
\qquad \text{(B-3)}
$$

From equation (B-3) it is clear that the time average is not an unbiased estimator of the brightness temperature. However, a closer look reveals that the time average is an unbiased estimate of the average brightness temperature of the scene covered by the antenna footprint in τ seconds.

If the time average is used as an estimator of the actual brightness temperature within the antenna footprint, a bias error will result. This bias error can be obtained by expanding the right side of equation (B-3) in a Taylor series. Performing this expansion about $\zeta = t$ results in

$$E\{\hat{\mu}_y(t)\} = \frac{1}{\tau}\int_{t-\tau/2}^{t+\tau/2} B(t) + (\zeta - t)B'(t) + \frac{(\zeta - t)^2}{2!}B''(t) + \frac{(\zeta - t)^3}{3!}B'''(t) + \ldots d\zeta$$

$$E\{\hat{\mu}_y(t)\} = B(t) + B'(t)\frac{1}{\tau}\int_{t-\tau/2}^{t+\tau/2}(\zeta - t)\,d\zeta + B''(t)\frac{1}{\tau}\int_{t-\tau/2}^{t+\tau/2}\frac{(\zeta - t)^2}{2!}d\zeta + \ldots \qquad \text{(B-4)}$$

$$E\{\hat{\mu}_y(t)\} = B(t) + B''(t)\frac{\tau^2}{24} + B''''(t)\frac{\tau^4}{1920}$$

$$E\{\hat{\mu}_y(t)\} = B(t) + \sum_{n=1}^{\infty}\frac{B^{(2n)}(t)\,\tau^{2n}}{(2n)!(2n+1)(2^{2n})}$$

where $B'(t)$ and $B^{(2n)}(t)$ represent the first and 2nth derivatives of $B(t)$ with respect to t respectively. The infinite sum of equation (B-4) is the resulting bias error if the time average is used as an estimate of $B(t)$. This bias error is due to the fact that the process is nonergodic.

1. Report No.	2. Government Accession No.	3. Recipient's Catalog No.
NASA TM-81932		

4. Title and Subtitle	5. Report Date
An Investigation of Radiometer Design Using Digital Processing Techniques	January 1981
	6. Performing Organization Code
7. Author(s)	8. Performing Organization Report No.
Roland W. Lawrence	
9. Performing Organization Name and Address	10. Work Unit No.
NASA Langley Research Center Hampton, VA 23665	506-61-33-31
	11. Contract or Grant No.
	13. Type of Report and Period Covered
12. Sponsoring Agency Name and Address	Technical Memorandum
National Aeronautics and Space Administration Washington, DC 20546	14. Sponsoring Agency Code

15. Supplementary Notes

16. Abstract

An investigation into the use of digital signal processing techniques in Dicke switching radiometer design is presented. The general approach of this investigation was to develop an analytical Model of the existing analog radiometer and identify factors which adversly affect its performance. A digital processor was then proposed to verify the feasibility of using digital techniques to minimize these adverse effects and improve the radiometer performance. Analysis and preliminary test results comparing the digital and analog signal processing approaches in radiometer design are then presented.

17. Key Words (Suggested by Author(s))	18. Distribution Statement
Radiometer Digital Processing Radiometer Dicke Noise Injection	Unclassified - Unlimited Subject Category 33

19. Security Classif. (of this report)	20. Security Classif. (of this page)	21. No. of Pages	22. Price*
Unclassified	Unclassified	100	

For sale by the National Technical Information Service, Springfield, Virginia 22161